Radiative corrections to leptonlepton scattering revisited

N Kaiser

Radiative corrections to lepton-lepton scattering revisited

N. Kaiser

Physik-Department T39, Technische Universität München, D-85747 Garching, Germany

Abstract

We calculate in closed analytical form the one-loop radiative corrections to electron-electron scattering $e^-e^- \to e^-e^-$. Explicit expressions (in terms of dimensionless Mandelstam variables) are given for the pertinent interference terms between the tree diagrams and the one-loop diagrams. Infrared finiteness of these virtual radiative corrections is achieved (in the standard way) by including soft photon radiation below an energy cut-off λ. We evaluate the remaining finite part of the soft photon correction factor in the center-of-mass frame. These results can be also utilized for Bhabha scattering $e^-e^+ \to e^-e^+$ and for elastic muon scattering $\mu^-\mu^\mp \to \mu^-\mu^\mp$. Furthermore, we calculate in the same way the one-loop radiative corrections to the scattering of unequal leptons $e^-\mu^- \to e^-\mu^-$ and apply them likewise to the muon pair production process $e^-e^+ \to \mu^+\mu^-$. In contrast to most other calculations of these radiative corrections we keep the full dependence on the lepton masses. Effects from hard photon radiation which are also important for a direct comparison with (a specific) experiment are not treated explicitly.

PACS: 12.20.-m, 12.20.Ds, 14.70.Bh

1 Introduction and summary

For a correct interpretation of the experimental data obtained in elastic or inelastic lepton scattering processes it is essential to include in the analysis of these data the radiative corrections arising from virtual photon loops and (soft) photon bremsstrahlung. Radiative corrections to electromagnetic processes have been first calculated in their classical works by Schwinger [1] for electron scattering in an external static potential, and by Brown and Feynman [2] for the Compton effect. Tsai [3] has extended the calculation of radiative corrections to elastic electron-proton scattering. The subject of radiative corrections has by now already a long history and we refer to the standard review papers of Maximon [4] and Mo and Tsai [5] which have been used in the interpretation of many electron scattering experiments. In recent years the issue of radiative corrections has received a renewed interest in connection with new precision experiments, performed e.g. at JLAB or MAMI. The two-photon exchange contribution [6, 7, 8] to the elastic electron-proton scattering plays in fact a crucial role in order to reconcile the apparent discrepancies for the ratio of the proton electric and magnetic form factors G_E^p/G_M^p as determined with the polarization transfer technique on the one hand side and via the (more traditional) Rosenbluth separation method on the other hand side. A comprehensive study of the analogous two-boson $(\gamma\gamma, \gamma Z^0)$ exchange corrections for parity-violating electron-proton scattering has been presented very recently in refs.[9, 10]. The complete treatment of the full excitation spectrum of the proton in the two-photon exchange remains still a challenge, and so far only the ground-state [7, 8] and the low-lying $\Delta^+(1232)$ resonance [11] have been taken into account in the computation of the respective two-photon exchange diagrams. Likewise, the QED radiative corrections to virtual Compton scattering off the proton $(e^-p \to e^-p\gamma)$ have been calculated and studied in ref.[12]. It has been concluded that a very good understanding of these radiative corrections is indispensable if one wants to extract nucleon structure information (such as generalized polarizabilities or generalized parton distributions) from the $e^-p \to e^-p\gamma$

reaction. Also recently, the radiative corrections to (real and virtual) pion Compton scattering have been calculated in refs.[13, 14]. These results are particularly relevant for analyzing the COMPASS experiment at CERN which aims at measuring the pion electric and magnetic polarizabilities (α_π and β_π) with high statistics using the Primakoff effect (i.e. the scattering of high-energy pions in the Coulomb field of a heavy nucleus).

The one-loop radiative corrections to the purely leptonic scattering process $e^-e^- \to e^-e^-$ have been calculated some time ago by Furlan and Peressutti in ref.[15]. However, as noted in their follow-up paper [16] on numerical results that original paper [15] contains some (unspecified) mistakes and misprints. A corrected version of their analytical formulas for the radiative corrections to electron-electron scattering has however never been published. The related paper by Tsai [17] deals only with the case of high-energy electron-electron scattering, where the radiative corrections can be approximated by some dominant logarithmic terms. Likewise, the one-loop radiative corrections to the scattering of unequal leptons, $e^-\mu^- \to e^-\mu^-$, have been calculated shortly afterwards by Eriksson in ref.[18]. Also in that case the original paper [18] contains mistakes and misprints which have been corrected iteratively in subsequent papers [19, 20] together with a presentation of some numerical results. Unfortunately, the comprehensibility of the analytical formulas written therein is not always straightforward since many auxiliary variables have been introduced although the process $e^-\mu^- \to e^-\mu^-$ can be described by just two independent Mandelstam variables. Moreover, it is rather cumbersome to trace back which part of the analytical expressions corresponds to a particular loop diagram.

In this situation it is still meaningful and helpful to reconsider the radiative corrections to lepton-lepton scattering. The purpose of the present paper is to document the results of such a careful rederivation. Our paper is organized as follows. In section 2, we calculate in closed analytical form the one-loop radiative corrections to electron-electron scattering $e^-e^- \to e^-e^-$. Explicit expressions (in terms of suitable dimensionless Mandelstam variables) are given for the pertinent interference terms between the tree diagrams and the one-loop diagrams summed over the electron spin states. Infrared finiteness of these virtual radiative corrections is achieved (in the standard way) by including soft photon radiation (off the in- or out-going electrons) below an energy cut-off λ. We evaluate the remaining finite part of the soft photon correction factor in the center-of-mass frame, assuming an isotropic photon emission therein. Figures with numerical results are presented in order to demonstrate the size as well as the energy and angular dependence of these radiative corrections to electron-electron scattering. By making use of crossing symmetry the radiative corrections to electron-positron (Bhabha) scattering $e^-e^+ \to e^-e^+$ can be obtained from the same analytical formulas. We consider also the elastic muon scattering processes $\mu^-\mu^\mp \to \mu^-\mu^\mp$ where the electronic vacuum polarization enters as a new and special feature. In section 3, we calculate then in the same way the one-loop radiative corrections to the scattering of unequal leptons $e^-\mu^- \to e^-\mu^-$. In that case the squared mass ratio $r = (m_e/m_\mu)^2$ comes into play as an additional parameter thus making the calculation a bit more challenging. After presenting numerical results for the radiative corrections to $e^-\mu^- \to e^-\mu^-$ scattering we turn via crossing symmetry to those for the muon pair production process $e^-e^+ \to \mu^+\mu^-$. For the purpose of comparison, we treat in section 4 the analogous radiative corrections for (point-like) charged scalar bosons. In the appendix, we collect the analytical results for the pertinent one-loop integrals with two, three and four propagators. We use dimensional regularization to treat both ultraviolet and infrared divergences (where the latter are caused by the vanishing photon mass). The imaginary parts of the loop functions are also given there. Together with a Kramers-Kronig dispersion relation these imaginary parts are most useful in order to control the correct analytical continuation of the real parts of the loop functions above their respective branch points.

In contrast to many other (modern) calculations of these QED radiative corrections we keep the full dependence on the lepton masses in all results. We do, however, not treat effects from

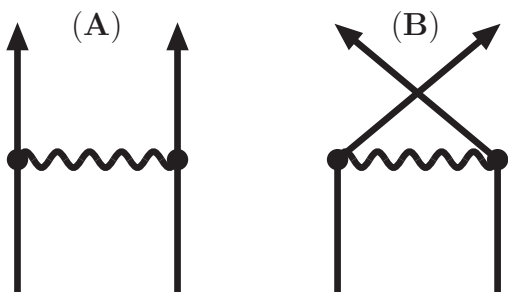

Figure 1: Tree diagrams, (A) and (B), for electron-electron scattering.

hard photon radiation or hadronic vacuum polarization, which can also be important for a (direct) comparison with experiments.

2 Radiative corrections to electron-electron scattering

We start out with calculating the radiative corrections to electron-electron scattering. The in- and out-going four-momenta of the reaction $e^-(p_1) + e^-(p_2) \to e^-(p_3) + e^-(p_4)$ give rise to the Lorentz-invariant (dimensionless) Mandelstam variables (s, t, u) defined as follows:

$$\begin{aligned} s\, m_e^2 &= (p_1 + p_2)^2 = (p_3 + p_4)^2\,, \\ t\, m_e^2 &= (p_1 - p_3)^2 = (p_2 - p_4)^2\,, \\ u\, m_e^2 &= (p_1 - p_4)^2 = (p_2 - p_3)^2\,. \end{aligned} \tag{1}$$

Since m_e^2 has been factored out they obey the numerical constraint $s + t + u = 4$, and in the physical region the inequalities $s > 4$, $t < 0$, $u < 0$ hold. In the case of unpolarized scattering the squared T-matrix for $e^-e^- \to e^-e^-$ has to be summed over all the electron spin-states. This fourfold sum is most efficiently performed via Dirac-traces: $\frac{1}{8}\mathrm{tr}[O_1(\not{p}_1 + m_e)\overline{O}_1(\not{p}_3 + m_e)]\cdot \mathrm{tr}[O_2(\not{p}_2 + m_e)\overline{O}_2(\not{p}_4 + m_e)]$ and $\frac{1}{8}\mathrm{tr}[O_1(\not{p}_1 + m_e)\overline{O}_1(\not{p}_4 + m_e)O_2(\not{p}_2 + m_e)\overline{O}_2(\not{p}_3 + m_e)]$. In order to keep the technical complications of the loop calculation as low as possible the integration over the loop-momenta in a photon-loop diagram is carried out after the summation over the electron spin-states. With that approach in mind the unpolarized differential cross section for electron-electron scattering in the center-of-mass frame, including radiative corrections of relative order α, can be represented in the following compact form:

$$\begin{aligned} \frac{d\sigma}{d\Omega_{\rm cm}} \;=\; \frac{\alpha^2}{2m_e^2 s}\Big\{ &\Big(\frac{A}{t} + \frac{B}{u}\Big) \otimes \Big(\frac{A}{t} + \frac{B}{u}\Big) \\ &+2\,\mathrm{Re}\Big[\Big(\mathrm{I} + \mathrm{II} + \mathrm{III} + \mathrm{IV}\Big) \otimes \Big(\frac{A}{t} + \frac{B}{u}\Big) + (t \leftrightarrow u)\Big]\Big\}\,, \end{aligned} \tag{2}$$

with $\alpha = 1/137.036$ the fine-structure constant. Here A and B denote the direct and crossed tree diagram (shown in Fig. 1) and I, II, III, IV stand for the four (classes of) contributing one-loop diagrams (shown in Figs. 2,3). The product symbol $\otimes$ designates the interference term between the T-matrices from two diagrams with the sums over the electron spins already carried out via Dirac-traces. The symmetrization prescription $+(t \leftrightarrow u)$ in eq.(2) generates the additional contributions from the crossed one-loop diagrams (i.e. the diagrams in Figs. 2,3 with crossed out-going electron lines).

The advantage of working with the dimensionless variables (t, u) shows up already when evaluating the Born terms. The two tree diagrams in Fig. 1 lead to the following simple polynomial expressions:

$$A \otimes A = t^2 + 2tu + 2(u-2)^2\,,$$

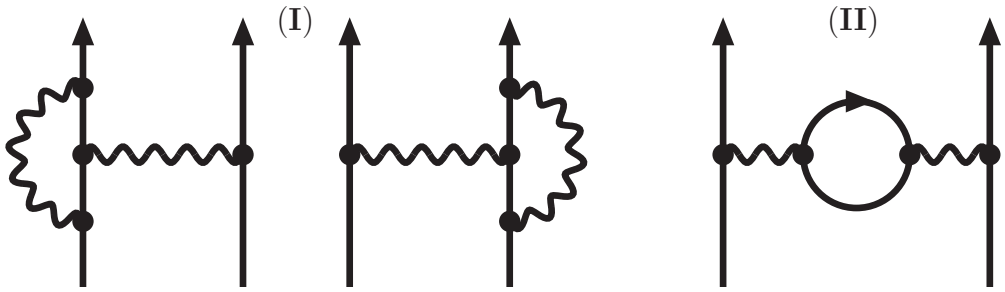

Figure 2: One-loop diagrams, (I) and (II), for electron-electron scattering.

$$A \otimes B = B \otimes A = (t+u)^2 - 4\,,$$
$$B \otimes B = 2(t-2)^2 + 2tu + u^2\,. \tag{3}$$

Note that the (relative) minus-sign belonging to the crossed tree diagram B, which originates from the exchange of two identical fermions, is already included in the interference term $A \otimes B = B \otimes A$. Specifying to the center-of-mass kinematics, $t = (4-s)(1-\cos\theta_{\rm cm})/2$ and $u = (4-s)(1+\cos\theta_{\rm cm})/2$ with $\theta_{\rm cm}$ the scattering angle,[1] the terms in the first line of eq.(2) produce the well-known Møller cross section for electron-electron scattering:

$$\frac{d\sigma^{(1\gamma)}}{d\Omega_{\rm cm}} = \frac{\alpha^2}{m_e^2 s}\left\{\frac{4(s-2)^2}{(s-4)^2}(4\eta^2-3\eta)+4\eta+1\right\}, \qquad \eta = \frac{1}{\sin^2\theta_{\rm cm}}\,. \tag{4}$$

2.1 Evaluation of one-loop diagrams

In this section, we present analytical expressions (of order α) for the interference terms between the one-loop diagrams and the tree diagrams for electron-electron scattering. We use dimensional regularization to treat both ultraviolet and infrared divergences (where the latter are caused by the masslessness of the photon). The method consists in calculating loop integrals in d spacetime dimensions and expanding the results around $d = 4$. Divergent pieces of one-loop integrals generically show up in form of the composite constant:

$$\xi = \frac{1}{d-4} + \frac{1}{2}(\gamma_E - \ln 4\pi) + \ln\frac{m_e}{\mu}\,, \tag{5}$$

containing a simple pole at $d = 4$. In addition, $\gamma_E = 0.5772\ldots$ is the Euler-Mascheroni number and μ an arbitrary mass scale introduced in dimensional regularization in order to keep the mass dimension of the loop integrals independent of d. Ultraviolet (UV) and infrared (IR) divergences are distinguished by the feature of whether the condition for convergence of the d-dimensional integral is $d < 4$ or $d > 4$. We discriminate them in the notation by putting appropriate subscripts, i.e. ξ_{UV} and ξ_{IR}. In order to simplify all calculations, we employ the Feynman gauge where the photon propagator is directly proportional to the Minkowski metric tensor $g^{\mu\nu}$. Let us now enumerate the analytical results as they emerge from the four (classes of) one-loop diagrams shown in Figs. 2,3.

The (on-shell) vertex corrections in both diagrams of class I are comprised by the one-photon loop form factors $F_{1,2}(t)^{\gamma-\rm loop}$ of the electron. These Dirac and Pauli form factors are normalized at zero momentum transfer $t = 0$ to: $F_1(0)^{\gamma-\rm loop} = 0$ and $F_2(0)^{\gamma-\rm loop} = \alpha/2\pi$ (anomalous magnetic moment). Putting all pieces together the pertinent interference terms with the (direct and crossed) tree diagrams read:

$$\mathrm{I} \otimes A \;=\; \frac{\alpha}{\pi t}\left\{\left[t^2+2tu+2(u-2)^2\right]\left\{\frac{t-2}{\sqrt{-t}\sqrt{4-t}}\left[4\xi_{IR}\sqrt{-t}\,L(-t)+\Phi(-t)\right]\right.\right.$$

[1] Since there are two identical particles in the final state the physical region is restricted to $0 < \theta_{\rm cm} \leq 90°$.

$$+2\xi_{IR}-2\Big\}+\frac{L(-t)}{\sqrt{4-t}}\Big[(4-t)(3t^2+16)+2u(8-3t)(t+u-4)\Big]\Big\}\,, \tag{6}$$

$$\begin{aligned}\mathrm{I}\otimes B &= \frac{\alpha}{\pi t}\Big\{\Big[(t+u)^2-4\Big]\Big\{\frac{t-2}{\sqrt{-t}\sqrt{4-t}}\Big[4\xi_{IR}\sqrt{-t}\,L(-t)+\Phi(-t)\Big]\\ &\quad +2\xi_{IR}-2\Big\}+\frac{L(-t)}{\sqrt{4-t}}\Big[3(4-t)(t+u)^2+2t^2-4u^2-32\Big]\Big\}\,.\end{aligned} \tag{7}$$

Here, we have introduced the frequently occurring logarithmic loop function:

$$L(x)=\frac{1}{\sqrt{x}}\ln\frac{\sqrt{4+x}+\sqrt{x}}{2}\,, \tag{8}$$

and the auxiliary function:

$$\Phi(x)=\mathrm{Li}_2(v(x))-\mathrm{Li}_2(1-v(x))+\frac{1}{2}\ln^2 v(x)-\frac{1}{2}\ln^2(1-v(x))\,, \tag{9}$$

composed of dilogarithms and squared logarithms of the argument:

$$v(x)=\frac{1}{2}\Big(1-\sqrt{\frac{x}{4+x}}\Big)\,, \tag{10}$$

where $\mathrm{Li}_2(v)=\sum_{n=1}^{\infty}n^{-2}v^n=v\int_1^\infty dy[y(y-v)]^{-1}\ln y$ denotes the conventional dilogarithmic function. Note that in addition to the photon-loop also the appropriate counterterm $Z_1-1=Z_2-1=\alpha(2\xi_{IR}+\xi_{UV}-2)/2\pi$ [12] of quantum electrodynamics which eliminates the ultraviolet divergence ξ_{UV} in the Dirac form factor $F_1(t)^{\gamma-\mathrm{loop}}$ has been included in eqs.(6,7).

Diagram II involves a vacuum polarization at the exchanged photon. Together with the counterterm $Z_3-1=2\alpha\,\xi_{UV}/3\pi$ [12] the contribution from the electronic vacuum polarization takes the form:

$$\mathrm{II}_e\otimes A=\frac{\alpha}{3\pi t^2}\Big[t^2+2tu+2(u-2)^2\Big]\Big\{(2t+4)\sqrt{4-t}\,L(-t)-\frac{5t}{3}-4\Big\}\,, \tag{11}$$

$$\mathrm{II}_e\otimes B=\frac{\alpha}{3\pi t^2}\Big[(t+u)^2-4\Big]\Big\{(2t+4)\sqrt{4-t}\,L(-t)-\frac{5t}{3}-4\Big\}\,. \tag{12}$$

The additional (small) effect from the muonic vacuum polarization at the exchanged photon is readily obtained by substituting $t\to rt$, with $r=(m_e/m_\mu)^2$ the squared mass ratio, in the polarization function:

$$\mathrm{II}_\mu\otimes A=\frac{\alpha}{3\pi t^2}\Big[t^2+2tu+2(u-2)^2\Big]\Big\{\Big(2t+\frac{4}{r}\Big)\sqrt{4-rt}\,L(-rt)-\frac{5t}{3}-\frac{4}{r}\Big\}\,, \tag{13}$$

$$\mathrm{II}_\mu\otimes B=\frac{\alpha}{3\pi t^2}\Big[(t+u)^2-4\Big]\Big\{\Big(2t+\frac{4}{r}\Big)\sqrt{4-rt}\,L(-rt)-\frac{5t}{3}-\frac{4}{r}\Big\}\,. \tag{14}$$

Next, we come to the (planar and crossed) two-photon exchange box diagrams shown in Fig. 3. For these diagrams it is most advantageous to perform the (multiple) spin sums via Dirac-traces before the (d-dimensional) loop-integration. In this way of proceeding the subsequent integrand emerges as a Lorentz-scalar constructed solely from the external four-momenta p_1,p_2,p_3,p_4 and the loop momentum l. It can be profitably decomposed into partial fractions, thus reducing greatly the number of independent loop integrals to be solved. All of these loop integrals are ultraviolet convergent but some of them generate additional infrared divergences

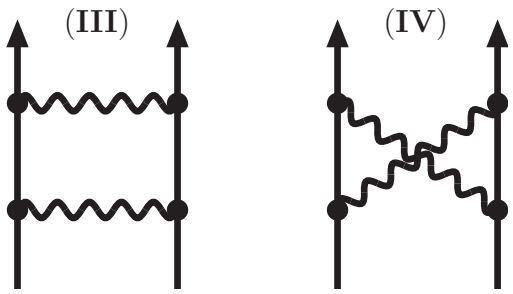

Figure 3: One-photon loop diagrams, (III) and (IV), for electron-electron scattering.

($\sim \xi_{IR}$). Employing the basic loop integrals $H(s)$, $K(t)$ and $\Psi(s,t)$ with three and four propagators, defined and solved in the appendix, one finds for the interference terms of the planar box diagram III with the tree diagrams the following analytical expressions:

$$\begin{aligned}
\mathrm{III}\otimes A &= \frac{\alpha}{\pi}\Bigg\{\Big[3t^2+6tu+4u^2-14t-24u+24+\frac{16u}{4-t}\Big]K(t)\\
&+\Big(\frac{4u}{4-t}-1-\frac{u}{2}\Big)\ln(-t)+\frac{L(-s)}{\sqrt{4-s}}(s^2+st-6s+8)\\
&+\frac{2-s}{\sqrt{4-s}}\,L(-s)\Big[\Big(3t+6u-8+\frac{4}{t}(u-2)^2\Big)\ln(-t)\\
&+4\xi_{IR}\Big(t+2u+\frac{2}{t}(u-2)^2\Big)\Big]+\frac{(2-s)(2s+t)}{2\sqrt{-s}\sqrt{4-s}}\,\Phi(-s)\Bigg\}, \qquad (15)\\
\mathrm{III}\otimes B &= \frac{\alpha}{\pi}\Bigg\{2\Big[(t+u)^2-t-2u-6+\frac{4u}{4-t}\Big]K(t)\\
&+\frac{2\,L(-s)}{\sqrt{4-s}}\Big[2u+\Big(\frac{6-s}{t}(s-2)^2-2s-u\Big)\ln(-t)\\
&+2\xi_{IR}\,\frac{6-s}{t}(s-2)^2\Big]+\frac{2u\ln(-t)}{4-t}+\frac{2s+u}{\sqrt{-s}\sqrt{4-s}}\,\Phi(-s)\Bigg\}, \qquad (16)
\end{aligned}$$

with the t-dependent auxiliary function:

$$K(t)=\frac{1}{\sqrt{-t}\sqrt{4-t}}\Big[\frac{\pi^2}{3}-t\,L^2(-t)+\mathrm{Li}_2\Big(\frac{2-t-\sqrt{-t}\sqrt{4-t}}{2}\Big)\Big]. \qquad (17)$$

In the same way one obtains for the interference terms of the crossed two-photon exchange box diagram IV with the tree diagrams the similar results:

$$\begin{aligned}
\mathrm{IV}\otimes A &= \frac{\alpha}{\pi}\Bigg\{\Big[8u-t^2-2tu-4u^2-2t-8+\frac{16u}{4-t}\Big]K(t)\\
&+\Big(\frac{4u}{4-t}-3+\frac{s}{2}\Big)\ln(-t)+\frac{L(-u)}{\sqrt{4-u}}(6u-tu-u^2-8)\\
&+\frac{u-2}{\sqrt{4-u}}\,L(-u)\Big[\Big(t+2u+\frac{4}{t}(u-2)^2\Big)\ln(-t)\\
&+4\xi_{IR}\Big(t+2u+\frac{2}{t}(u-2)^2\Big)\Big]+\frac{(u-2)(t+2u)}{2\sqrt{-u}\sqrt{4-u}}\,\Phi(-u)\Bigg\}, \qquad (18)\\
\mathrm{IV}\otimes B &= \frac{\alpha}{\pi}\Bigg\{\Big[4-t^2-2tu-2u^2-4u+\frac{8u}{4-t}\Big]K(t)
\end{aligned}$$

$$
\begin{aligned}
&+\frac{L(-u)}{\sqrt{4-u}}\Big[4\xi_{IR}\,(u-2)\Big(t+2u+\frac{u^2-4}{t}\Big)+(2-t)(4+u)\\
&-u^2+\Big(tu+2u^2-6u-8+\frac{2}{t}(u+2)(u-2)^2\Big)\ln(-t)\Big]\\
&+\Big(\frac{2u}{4-t}-1+\frac{s}{2}\Big)\ln(-t)+\frac{2u^2+(4-u)(2-t)}{2\sqrt{-u}\sqrt{4-u}}\,\Phi(-u)\Big\}\,. \qquad (19)
\end{aligned}
$$

We note that it is instrumental to keep the factorized square roots in eqs.(6-19) as they stand. If one would combine them into a single square root than a wrong sign could be obtained for some terms. We have checked via the Kramers-Kronig dispersion relation and the imaginary parts of the loop functions (given in the appendix) that the factorized square roots lead in all cases to the correct analytical continuation of the (only relevant) real parts of the loop functions along their branch cuts. When written with factorized square roots the correct sign often emerges as $i \cdot i = -1$ from two negative radicands. It is important to have a representation with the correct analytical continuation built in, if one wants to carry over the results of the loop calculation from electron-electron scattering to electron-positron scattering (via the crossing transformation $s \leftrightarrow u$).

2.2 Infrared finiteness and numerical results

In the next step we have to consider the infrared divergent terms proportional to ξ_{IR}. Inspection of eqs.(6,7,15,16,18,19) reveals that these scale with the Born terms $A\otimes A/t$ and $A\otimes B/t$ given in eq.(3). As a consequence of that feature, the infrared divergent loop corrections multiply the differential cross section $d\sigma^{(1\gamma)}/d\Omega_{\rm cm}$ at leading order by a ($t \leftrightarrow u$ crossing-symmetric) factor:

$$
\delta^{(IR)}_{\rm virt} = \frac{8\alpha}{\pi}\,\xi_{IR}\left\{\frac{1}{2}+\frac{t-2}{\sqrt{4-t}}L(-t)+\frac{u-2}{\sqrt{4-u}}L(-u)+{\rm Re}\Big[\frac{2-s}{\sqrt{4-s}}L(-s)\Big]\right\}. \qquad (20)
$$

The unphysical infrared divergence ξ_{IR} gets canceled at the level of the (measurable) cross section by the contributions from soft photon bremsstrahlung. In its final effect, the (single) soft photon radiation off the in- or out-going electrons multiplies the Møller cross section $d\sigma^{(1\gamma)}/d\Omega_{\rm cm}$ by a factor:

$$
\begin{aligned}
\delta_{\rm soft} \;=\; & \alpha\,\mu^{4-d}\int\limits_{|\vec{l}|<\lambda}\frac{d^{d-1}l}{(2\pi)^{d-2}\,l_0}\Big\{\frac{2p_1\cdot p_3}{p_1\cdot l\,p_3\cdot l}+\frac{2p_2\cdot p_4}{p_2\cdot l\,p_4\cdot l}+\frac{2p_1\cdot p_4}{p_1\cdot l\,p_4\cdot l}+\frac{2p_2\cdot p_3}{p_2\cdot l\,p_3\cdot l}\\
&-\frac{2p_1\cdot p_2}{p_1\cdot l\,p_2\cdot l}-\frac{2p_3\cdot p_4}{p_3\cdot l\,p_4\cdot l}-\frac{m_e^2}{(p_1\cdot l)^2}-\frac{m_e^2}{(p_2\cdot l)^2}-\frac{m_e^2}{(p_3\cdot l)^2}-\frac{m_e^2}{(p_4\cdot l)^2}\Big\}, \qquad (21)
\end{aligned}
$$

which depends on a small photon energy cut-off λ. Working out this momentum space integral by the method of dimensional regularization (with $d > 4$) one finds that the infrared divergent correction factor $\delta^{(\rm IR)}_{\rm virt} \sim \xi_{IR}$ in eq.(20) gets eliminated and the following finite radiative correction factor remains:

$$
\begin{aligned}
\delta^{(\rm cm)}_{\rm real} \;=\; & \frac{2\alpha}{\pi}\Big\{4\Big[\frac{1}{2}+\frac{t-2}{\sqrt{4-t}}L(-t)+\frac{u-2}{\sqrt{4-u}}L(-u)+\frac{s-2}{\sqrt{s}}L(s-4)\Big]\ln\frac{m_e}{2\lambda}\\
&+2\sqrt{s}\,L(s-4)+\int_0^{1/2}dx\Big\{\frac{\sqrt{s}(t-2)}{[1-tx(1-x)]W_t}\ln\frac{\sqrt{s}+W_t}{\sqrt{s}-W_t}\\
&+\frac{\sqrt{s}(u-2)}{[1-ux(1-x)]W_u}\ln\frac{\sqrt{s}+W_u}{\sqrt{s}-W_u}\Big\}+\frac{2s-4}{\sqrt{s^2-4s}}\Big[(4-s)\,L^2(s-4)\\
&+\sqrt{s-4}\,\ln(s-4)\,L(s-4)+\frac{\pi^2}{6}-{\rm Li}_2\Big(\frac{s-2-\sqrt{s^2-4s}}{2}\Big)\Big]\Big\}, \qquad (22)
\end{aligned}
$$

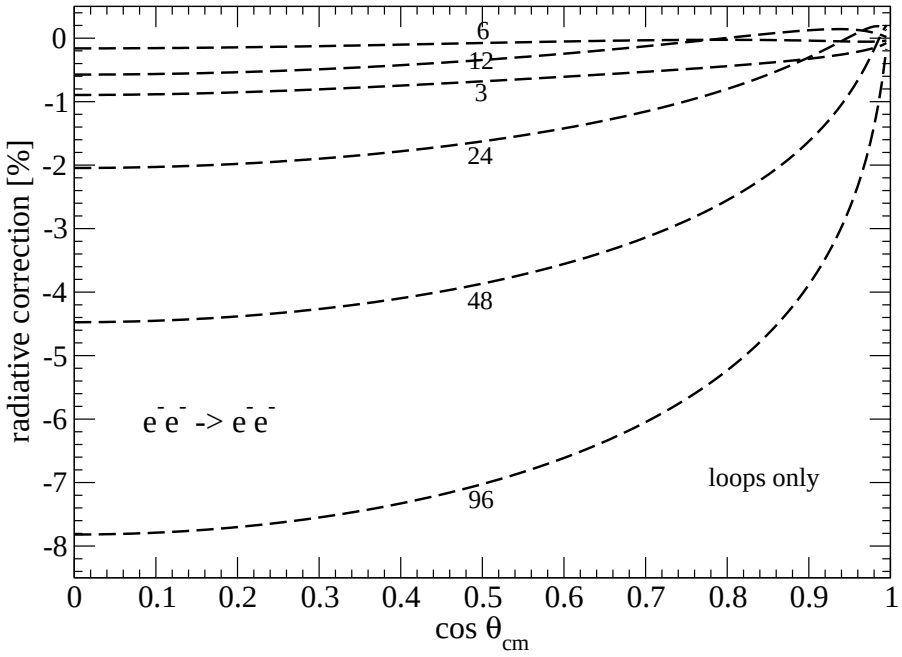

Figure 4: Radiative corrections to electron-electron scattering arising from loops only. The numbers $(3, 6, 12, 24, 48, 96)$ on the curves correspond to the total center-of-mass energy $\sqrt{s}m_e$ in units of m_e.

with the abbreviations $W_t = \sqrt{s - 4 + 4tx(1-x)}$ and $W_u = \sqrt{s - 4 + 4ux(1-x)}$. We remark that the exact cancellation of infrared divergences ξ_{IR} works out by reason of the identity: $\mathrm{Re}\,[(2-s)L(-s)/\sqrt{4-s}\,] = (s-2)L(s-4)/\sqrt{s}$, where the sign change emerges from two negative radicands. Furthermore, we note that the terms beyond those proportional to $\ln(m_e/2\lambda)$ are specific for the evaluation of the soft photon correction factor δ_{soft} in the center-of-mass frame with λ an infrared cut-off therein. As it is written in eq.(22), $\delta_{\mathrm{real}}^{(\mathrm{cm})}$ refers to an (idealized) experimental situation where all undetected soft photon radiation fills a small sphere of radius λ in the center-of-mass frame. In a real experiment the momentum space region of undetected photons can be of different (e.g. non-isotropic) shape with no sharp boundaries due to detector efficiencies etc. Such additional experiment specific radiative corrections can be accounted for and calculated by integrating the fivefold differential cross section for $e^-e^- \to e^-e^-\gamma$ over the appropriate region in phase space. By construction this region excludes the infrared singular domain $|\vec{l}\,| < \lambda$ and thus leads to a finite result. At this point one should note that for comparison with a real experiment the treatment of hard photon bremsstrahlung is also important.

We are now in the position to present some numerical results for the radiative corrections to electron-electron scattering $e^-e^- \to e^-e^-$. The radiative correction factor is $\delta_{\mathrm{real}}^{(\mathrm{cm})}$ written in eq.(22) plus the sum of all finite interference terms (second line in eq.(2) with $\xi_{IR} \to 0$) divided by the Born terms (first line in eq.(2)). Fig. 4 shows in percent the radiative corrections arising from loops alone (discarding the infrared divergent ξ_{IR} terms) at seven selected center-of-mass energies $\sqrt{s}m_e = (3,\ 6,\ 12,\ 24,\ 48,\ 96)m_e$. One notices that these (mostly negative) photon-loop corrections become maximal for perpendicular scattering ($\theta_{\mathrm{cm}} = 90^\circ$) and that they grow approximately linearly with the total center-off-mass energy $\sqrt{s}m_e$. The effect from the muonic vacuum polarization (see eqs.(13,14)) is negligibly small in the energy range considered. Let us also mention that we confirm with good accuracy the numerical results of Furlan and Peressutti presented in ref.[16]. The full lines in Fig. 5 show the radiative corrections to electron-electron scattering with inclusion of the soft photon bremsstrahlung. For the sake of having a concrete case we have set the infrared cutoff to the value $\lambda = \sqrt{s}m_e/200$, thus modelling an (idealized)

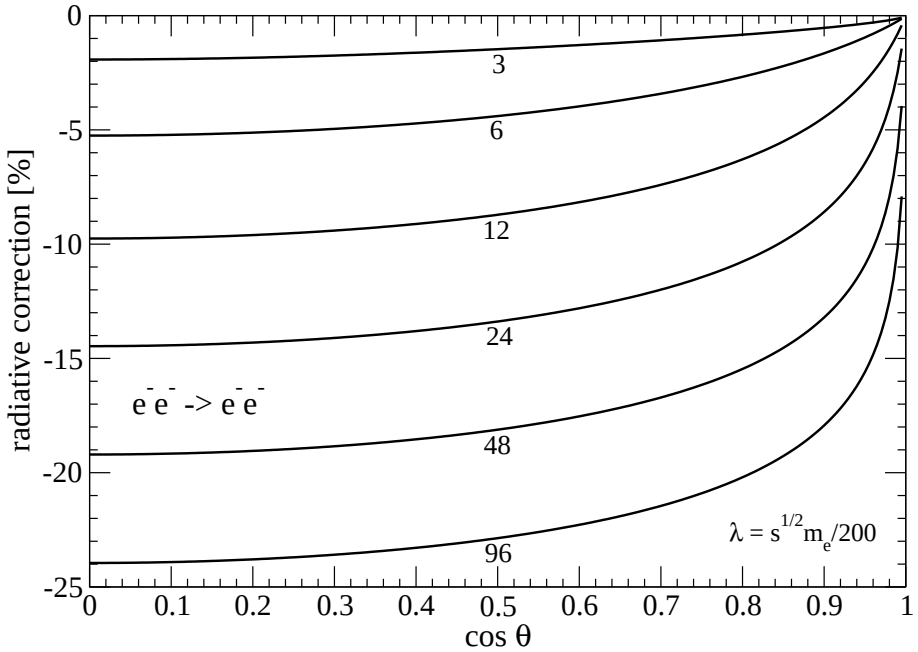

Figure 5: Radiative corrections to electron-electron scattering including soft photon bremsstrahlung. The numbers $(3, 6, 12, 24, 48, 96)$ on the curves correspond to the total center-of-mass energy $\sqrt{s}m_e$ in units of m_e. The infrared cutoff has been set to $\lambda = \sqrt{s}m_e/200$.

experimental situation where the electron energies can be resolved within 1% accuracy. One observes that the soft photon bremsstrahlung significantly increases the (negative) radiative corrections to electron-electron scattering. An approximate logarithmic scaling with the total center-off-mass energy $\sqrt{s}m_e$ can now be recognized. Similar features apply also to the radiative corrections to (electron and pion) Compton scattering [2, 13]. Clearly, as soon as the order α radiative corrections exceed about 20% in magnitude one has to worry about the two-loop and double bremsstrahlung effects of order α^2. At higher energies the hadronic vacuum polarization will even start to play a role. Pursuing such higher order and heavy mass effects goes beyond the scope of the present work.

2.3 Radiative corrections to Bhabha scattering

Next, we want to discuss the radiative corrections to electron-positron (Bhabha) scattering. The reaction $e^-e^+ \to e^-e^+$ can be obtained from electron-electron $e^-(p_1)+e^-(p_2) \to e^-(p_3)+e^-(p_4)$ via the replacement $p_2 \leftrightarrow -p_4$ of in- and out-going four-momenta. In terms of the invariant Mandelstam variables this involves the crossing transformation $s \leftrightarrow u$. The crossed one-photon exchange diagram B in Fig. 1 gets this way converted into the annihilation diagram. At leading order the Bhabha cross section takes the form:

$$\frac{d\sigma^{(e^-e^+)}}{d\Omega_{\rm cm}} = \frac{\alpha^2}{m_e^2 s}\Big\{\frac{(s-2)^2}{(s-4)^2\,\zeta^2} + \frac{4-2s^2}{s(s-4)\,\zeta} + 2 + \frac{4}{s} + \frac{1}{s^2}\Big[s-2+(4-s)\,\zeta\Big]^2\Big\}\,, \qquad (23)$$

where $\zeta = \sin^2(\theta_{\rm cm}/2)$ with $\theta_{\rm cm}$ the scattering angle in the center-of-mass frame. Note that there is missing a factor $1/4$ in the second term in eq.(6.47) of the textbook by Itzykson and Zuber [21].

While the results for the one-loop corrections to electron-positron scattering can be directly taken over from subsection 2.1 via the substitution $s \leftrightarrow u$ this does not hold in the same way for the contributions from the soft photon bremsstrahlung. In the reaction $e^-e^+ \to e^-e^+$ the soft photon is emitted either from a negatively or positively charged particle and this leads to

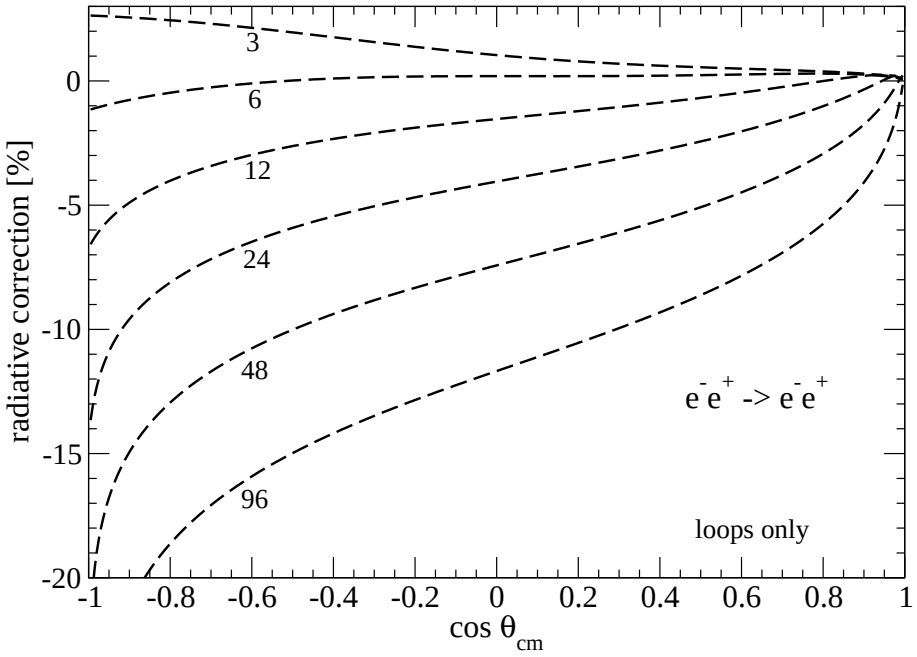

Figure 6: Radiative corrections to electron-positron scattering arising from loops only. The numbers $(3, 6, 12, 24, 48, 96)$ on the curves correspond to the total center-of-mass energy $\sqrt{s}$ in units of m_e.

a sign change in some (quantum mechanical) interference terms. In comparison to eq.(22) the s and u dependent interference terms change sign and (after cancelling the infrared divergence ξ_{IR}) the finite part of the soft photon correction factor for electron-positron scattering reads:

$$\begin{aligned}
\delta_{\rm real}^{(\rm cm)} \;=\; & \frac{2\alpha}{\pi}\Bigg\{4\Big[\frac{1}{2}+\frac{t-2}{\sqrt{4-t}}L(-t)+\frac{2-u}{\sqrt{4-u}}L(-u)+\frac{2-s}{\sqrt{s}}L(s-4)\Big]\ln\frac{m}{2\lambda} \\
& +2\sqrt{s}\,L(s-4)+\int_0^{1/2}dx\Big\{\frac{\sqrt{s}(t-2)}{[1-tx(1-x)]W_t}\ln\frac{\sqrt{s}+W_t}{\sqrt{s}-W_t} \\
& +\frac{\sqrt{s}(2-u)}{[1-ux(1-x)]W_u}\ln\frac{\sqrt{s}+W_u}{\sqrt{s}-W_u}\Big\}+\frac{2s-4}{\sqrt{s^2-4s}}\Big[(s-4)\,L^2(s-4) \\
& -\sqrt{s-4}\,\ln(s-4)\,L(s-4)-\frac{\pi^2}{6}+{\rm Li}_2\Big(\frac{s-2-\sqrt{s^2-4s}}{2}\Big)\Big]\Bigg\}. \qquad (24)
\end{aligned}$$

Let us clarify instantaneously that no further $s \leftrightarrow u$ crossing must be applied to the soft photon correction factor written in eq.(23). Returning to eq.(20) with permuted variables $s \leftrightarrow u$ one finds that now the exact cancellation of infrared divergences ξ_{IR} works out by reason of the identity: $\mathrm{Re}\,[(s-2)L(-s)/\sqrt{4-s}\,] = (2-s)L(s-4)/\sqrt{s}$.

The dashed lines in Fig. 6 show in percent the radiative corrections to electron-positron scattering arising from (photon and electron-positron) loops only. In comparison to electron-electron scattering (see Fig. 4) the size of these radiative corrections has significantly increased, in particular for scattering under backward angles, $90^\circ < \theta_{\rm cm} < 180^\circ$. Let us also mention that we confirm the numerical results of Furlan and Peressutti presented in ref.[16]. The full lines in Fig. 7 show the radiative corrections to electron-positron scattering with inclusion of the soft photon bremsstrahlung. The infrared cut-off has been set to the value $\lambda = \sqrt{s}m_e/200$, with the intension to model an (idealized) experimental situation where the electron and positron energies can be resolved within 1% accuracy. It is evident from Fig. 7 that the soft photon bremsstrahlung effects, which have not been considered by Furlan and Peressutti in ref.[16], add sizeably to the radiative corrections to electron-positron scattering.

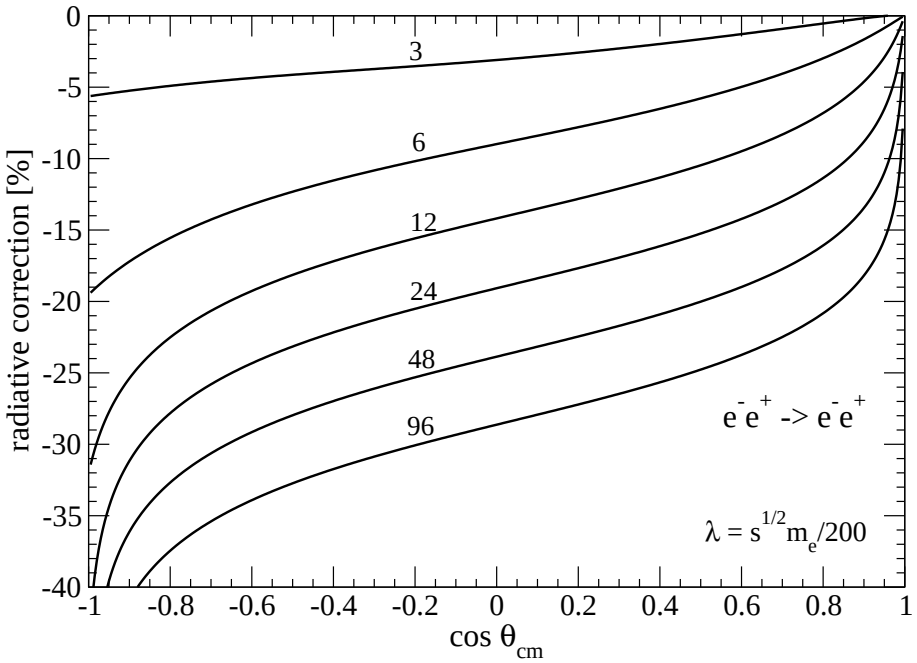

Figure 7: Radiative corrections to electron-positron scattering including soft photon bremsstrahlung. The numbers $(3, 6, 12, 24, 48, 96)$ on the curves correspond to the total center-of-mass energy $\sqrt{s}$ in units of m_e. The infrared cutoff has been set to $\lambda = \sqrt{s}m_e/200$.

It should again be stressed that for a comparison with real experiments the hard photon contributions also have to be included. Generally, the hard bremsstrahlung is not cut completely, but treated as part of the QED radiative corrections. We do not pursue these (experiment-specific) contributions here further. As a consequence of that omission the numerical results presented in all figures should be considered only as indicative.

Let us comment on some recent related works. In the work by Fleischer et al. [22] the one-loop photonic corrections to Bhabha scattering have been calculated in d spacetime dimensions. We have checked our results against theirs and found in the case $d = 4$ satisfactory agreement for all calculated terms. Actually, the two-loop radiative corrections to high-energy Bhabha scattering (approximated by the dominant logarithms in the electron mass m_e) are also known by now from the work of Penin [23]. We find that in the low-energy region considered here the subleading effects in the lepton mass still play a role.

2.4 Radiative corrections to elastic muon scattering

Having available the analytical results for the one-loop radiative corrections to electron-electron (and electron-positron) scattering one can furthermore apply them to the elastic muon scattering processes $\mu^-\mu^\mp \to \mu^-\mu^\mp$. Only the role of the electron and the muon needs to be interchanged (via the substitution of masses $m_e \leftrightarrow m_\mu$) in the analytical expressions presented so far. The electronic vacuum polarization to the photon-exchange given accordingly by eqs.(13,14) is now written in terms of the large variable $t/r = t(m_\mu/m_e)^2 = 42753\,t$. Despite that huge enhancement factor the effect of the electronic vacuum polarization is rather modest because of its weak (asymptotic) logarithmic t/r dependence. The estimate $-(2\alpha/3\pi)\ln r \simeq 1.65\%$ suggests a positive contribution of the order of a few percent from the electronic vacuum polarization in elastic muon scattering. This expectation is confirmed by the curves in Figs. 8,9 which show the calculated radiative corrections to $\mu^-\mu^- \to \mu^-\mu^-$ and $\mu^-\mu^+ \to \mu^-\mu^+$ scattering. In order to be comparable with the electron case the infrared cut-off for soft photon bremsstrahlung has been set now to the value $\lambda = \sqrt{s}m_\mu/200$. Indeed one finds by comparison with Figs. 5,7 that

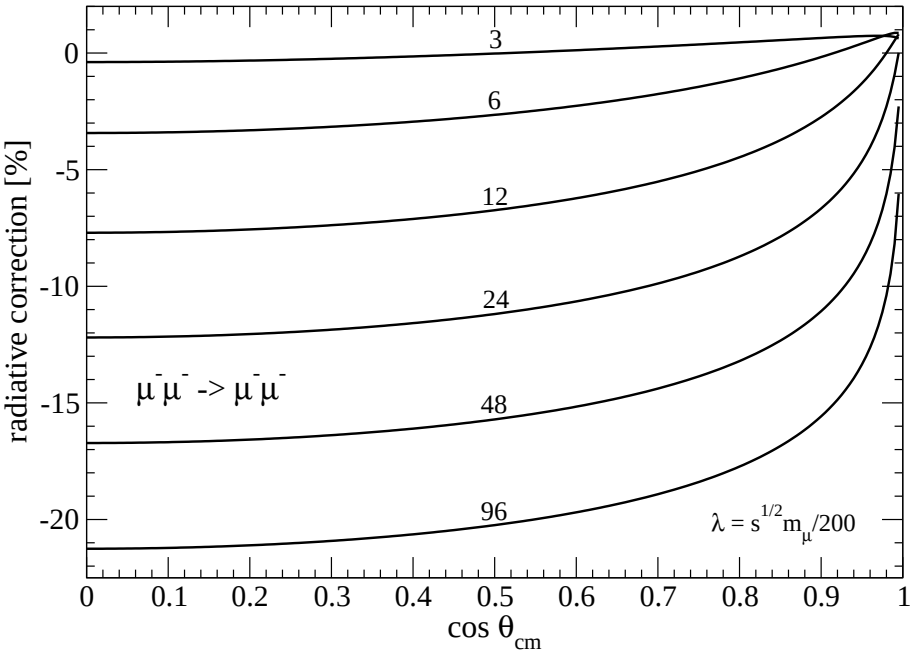

Figure 8: Radiative corrections to elastic muon scattering $\mu^-\mu^- \to \mu^-\mu^-$. The numbers $(3, 6, 12, 24, 48, 96)$ on the curves correspond to the total center-of-mass energy $\sqrt{s}m_\mu$ in units of m_μ. The infrared cutoff has been set to $\lambda = \sqrt{s}m_\mu/200$.

the curves in Figs. 8,9 are shifted upwards by a few percent. This shift grows approximately as $(2\alpha/3\pi)\ln(s/r)$ with the total center-of-mass energy $\sqrt{s}m_\mu$.

3 Radiative corrections to electron-muon scattering

In this section, we calculate the one-loop radiative corrections to the scattering of unequal leptons (e.g. electrons and muons). The in- and out-going four-momenta of the reaction $e^-(p_1) + \mu^-(p_2) \to e^-(p_3) + \mu^-(p_4)$ give rise to the (dimensionless) Mandelstam variables: $s = (p_1 + p_2)^2/m_\mu^2$, $t = (p_1 - p_3)^2/m_\mu^2$, $u = (p_1 - p_4)^2/m_\mu^2$, where we have divided by the square of the (large) muon mass m_μ^2. These convenient dimensionless variables satisfy the constraint $s + t + u = 2 + 2r$ with $r = (m_e/m_\mu)^2$ the squared mass ratio. In analogy to eq.(2) the unpolarized differential cross section for electron-muon scattering ($e^-\mu^- \to e^-\mu^-$) in the center-of-mass frame, including radiative corrections of relative order α, takes the following form:

$$\frac{d\sigma^{(e^-\mu^-)}}{d\Omega_{\rm cm}} = \frac{\alpha^2}{2m_\mu^2 s}\left\{\frac{A' \otimes A'}{t^2} + \frac{2}{t}\,\mathrm{Re}\Big[(\mathrm{I}' + \mathrm{II}' + \mathrm{III}' + \mathrm{IV}') \otimes A'\Big]\right\}. \tag{25}$$

The momentum transfer variable t is given as $t = [s^2 - 2s(1+r) + (1-r)^2](\cos\theta_{\rm cm} - 1)/2s$ in terms of the center-of-mass scattering angle $\theta_{\rm cm}$ and the total center-of-mass energy $\sqrt{s}m_\mu$.

In the case of unequal lepton scattering only the direct photon exchange diagram A' (see Fig. 1) is possible and the corresponding spin-summed Born term reads:

$$A' \otimes A' = 2(s-1-r)^2 + 2st + t^2 = 2(u-1-r)^2 + 2ut + t^2\,. \tag{26}$$

Note the invariance of $A' \otimes A'$ under the crossing transformation $s \leftrightarrow u$. It expresses the obvious fact that at leading order the cross sections for $e^-\mu^- \to e^-\mu^-$ and $e^-\mu^+ \to e^-\mu^+$ are equal. In eq.(25), I′, II′, III′, IV′ stand for the four (classes of) loop diagrams shown in Fig. 2,3 interpreted now as diagrams for electron-muon scattering. By the prime ′ we distinguish them notationally from those for electron-electron scattering. The product symbol $\otimes$ designates

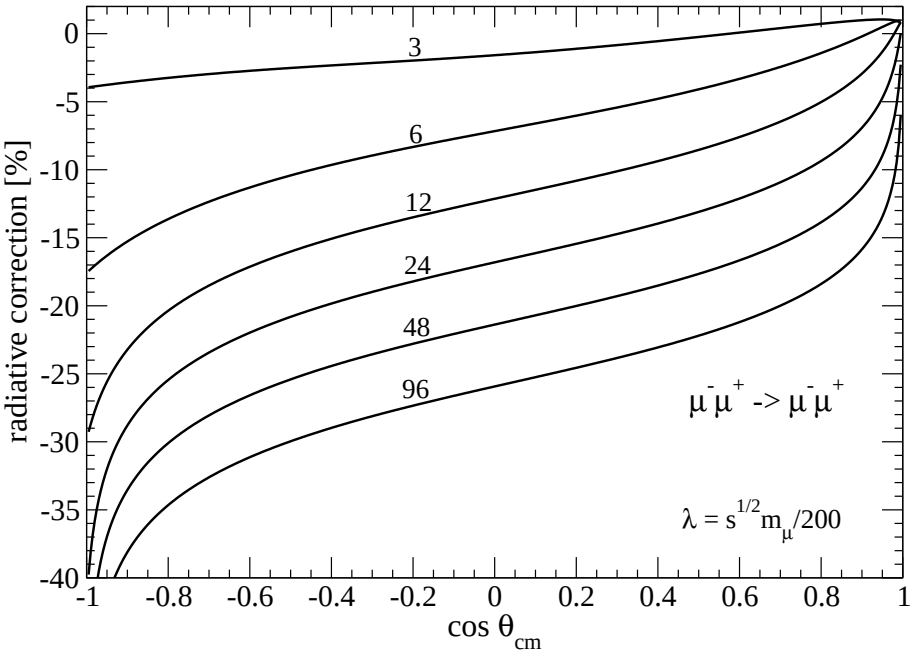

Figure 9: Radiative corrections to muonic Bhabha scattering $\mu^-\mu^+ \to \mu^-\mu^+$. The numbers $(3, 6, 12, 24, 48, 96)$ on the curves correspond to the total center-of-mass energy $\sqrt{s}m_\mu$ in units of m_μ. The infrared cutoff has been set to $\lambda = \sqrt{s}m_\mu/200$.

again the interference term between the T-matrices from two diagrams with the sums over electron and muon spins already carried out via Dirac-traces: $\frac{1}{8}\mathrm{tr}[O_1(\not{p}_1 + m_e)\overline{O}_1(\not{p}_3 + m_e)]\cdot \mathrm{tr}[O_2(\not{p}_2 + m_\mu)\overline{O}_2(\not{p}_4 + m_\mu)]$.

3.1 Evaluation of one-loop diagrams

In this subsection we present analytical expressions (of order α) for the interference terms between the one-loop diagrams and the tree diagram A' for electron-muon scattering.

Considering the diagrams of class I′ shown in Fig. 2 one can have a vertex correction either at the (left) electron line or at the (right) muon line. In both cases it is given by the respective one-photon loop form factors $F_{1,2}^{\gamma-\mathrm{loop}}(t)$ for electrons or muons. The pertinent interference term of the electronic vertex correction with the tree diagram A' takes the form:

$$\begin{aligned} \mathrm{I}'_e \otimes A' \;=\; & \frac{\alpha}{2\pi t}\Big\{ A' \otimes A' \Big[\frac{L(-tr^{-1})}{\sqrt{4r^2 - rt}} \Big((4\xi_{IR} + 2\ln r)(t - 2r) + 8r - 3t \Big) \\ & + \frac{(t - 2r)\Phi(-tr^{-1})}{\sqrt{-t}\sqrt{4r - t}} + 2\xi_{IR} - 2 + \ln r \Big] + 4t\sqrt{r}(2 + t)\frac{L(-tr^{-1})}{\sqrt{4r - t}} \Big\}, \end{aligned} \tag{27}$$

while that of muonic vertex correction reads:

$$\begin{aligned} \mathrm{I}'_\mu \otimes A' \;=\; & \frac{\alpha}{2\pi t}\Big\{ A' \otimes A' \Big[\frac{L(-t)}{\sqrt{4 - t}} \Big(4\xi_{IR}(t - 2) + 8 - 3t \Big) \\ & + \frac{(t - 2)\Phi(-t)}{\sqrt{-t}\sqrt{4 - t}} + 2\xi_{IR} - 2 \Big] + 4t(2r + t)\frac{L(-t)}{\sqrt{4 - t}} \Big\}. \end{aligned} \tag{28}$$

Note that the infrared divergence ξ_{IR} (see eq.(5)) is now redefined with the muon mass m_μ under the logarithm $\ln(m_\mu/\mu)$. This leads to the additional $\ln r$ terms for $\mathrm{I}'_e \otimes A'$ written in eq.(27). The functions $L(-t)$ and $\Phi(-t)$ have been defined in eqs.(8,9,10).

The vacuum polarization diagram II′ shown in Fig. 2 comes also in two versions, either as electronic vacuum polarization:

$$\mathrm{II}'_e \otimes A' = \frac{\alpha}{3\pi t^2}\left\{\frac{2}{\sqrt{r}}(t+2r)\sqrt{4r-t}\,L(-tr^{-1}) - \frac{5t}{3} - 4r\right\} A' \otimes A'\,, \tag{29}$$

or as muonic vacuum polarization:

$$\mathrm{II}'_\mu \otimes A' = \frac{\alpha}{3\pi t^2}\left\{(2t+4)\sqrt{4-t}\,L(-t) - \frac{5t}{3} - 4\right\} A' \otimes A'\,. \tag{30}$$

More tedious to evaluate are the (planar and crossed) two-photon exchange box diagrams shown in Fig. 3. We take advantage of performing first the spin-sums (via Dirac-traces) and of decomposing in the next step the resulting Lorentz-scalar loop integrand into partial fractions. In this form the majority of terms has either only one electron propagator or only one muon propagator and few terms involve the product of both. The latter loop integrals depend in a non-trivial way on the squared mass ratio $r = (m_e/m_\mu)^2$. Putting all pieces together one finds for the interference term of the planar two-photon exchange diagram III′ with the tree diagram A' the following analytical expression:

$$\begin{aligned}
\mathrm{III}' \otimes A' \;=\; & \frac{\alpha}{\pi}\Bigg\{\left[\frac{8}{4-t}(r-1-s) + \frac{t^2}{2} + t + st + 2(s-r)^2 + 2\right] K(t) \\
& + \left[\frac{8r}{4r-t}(1-r-s) + \frac{t^2}{2r} + \frac{t}{r}(s+r) + \frac{2}{r}(s-1)^2 + 2r\right] K(tr^{-1}) \\
& + \left[\frac{2}{4-t}(r-1-s) + \frac{2r}{4r-t}(1-r-s) + \frac{1}{2}(s+t+1+r)\right]\ln(-t) \\
& + \left[\frac{r-1}{s}(1+r+t) + \frac{8r}{4r-t}(s+r-1) + 2 - 4r - s - t\right]\frac{\ln r}{4} \\
& + \frac{1+r-s}{\sqrt{\rho_+ - s}\sqrt{\rho_- - s}}\left[4\xi_{IR}\left(2s + t + \frac{2}{t}(s-1-r)^2\right)\right. \\
& \left. + \left(2s + t + \frac{4}{t}(s-1-r)^2\right)\ln(-t)\right]\ln\frac{\sqrt{\rho_+ - s} + \sqrt{\rho_- - s}}{2r^{1/4}} \\
& + \left[s^2 + st - 3s(1+r) + 3r^2 + 2r + 3 - \frac{(1-r)^2}{s}(1+r+t)\right] \\
& \times \frac{1}{\sqrt{\rho_+ - s}\sqrt{\rho_- - s}}\ln\frac{\sqrt{\rho_+ - s} + \sqrt{\rho_- - s}}{2r^{1/4}} + \frac{1}{2}(2s+t) \\
& \times (1+r-s)\int_{\rho_+}^{\infty} dx \frac{\ln[x - 2 - 2r + (1-r)^2 x^{-1}]}{\sqrt{x^2 - 2x(1+r) + (1-r)^2}\,(x-s)}\Bigg\}\,,
\end{aligned} \tag{31}$$

with the abbreviations $\rho_\pm = 1 + r \pm 2\sqrt{r}$. For the numerical evaluation of the (only relevant) real part of $\mathrm{III}' \otimes A'$ the spectral integral $\int_{\rho_+}^{\infty} dx/(x-s)\ldots$ in the last line of eq.(31) has to be treated as a principal value integral (if $s > \rho_+$). It can be conveniently decomposed into a sum of two non-singular integrals by the following formula:

$$⨍_{\rho_+}^{\infty} dx\,\frac{f(x)}{x-s} = \int_{\rho_+}^{2s-\rho_+} dx\,\frac{f(x)-f(s)}{x-s} + \int_{2s-\rho_+}^{\infty} dx\,\frac{f(x)}{x-s}\,. \tag{32}$$

Finally, we are left with the contribution of the crossed two-photon exchange box diagram IV′ shown in Fig. 3. Its interference term with the tree diagram A' can be obtained via crossing $(s \to u = 2 + 2r - s - t)$ as follows:[2]

$$\mathrm{IV}' \otimes A' = -\mathrm{III}' \otimes A'\,|_{s\to u}\,, \tag{33}$$

[2]Because of this property all the s-independent terms in the first four lines of eq.(31) could be dropped without affecting the sum $(\mathrm{III}' + \mathrm{IV}') \otimes A'$.

with III$'\otimes A'$ given in eq.(31). We have actually verified this relation by an explicit calculation of IV$'\otimes A'$ as it arises from the crossed two-photon exchange diagram IV$'$. The physical reason behind eq.(33) can be easily explained and understood. When turning the right muon line in the crossed two-photon exchange diagram IV$'$ upside-down one gets the planar two-photon exchange diagram III$'$ for electron-antimuon scattering ($e^-\mu^+ \to e^-\mu^+$). The same manipulation applied to the tree diagram A' introduces an additional minus sign due to the (single) opposite electric charge, and to close the argument, $e^-\mu^+ \to e^-\mu^+$ and $e^-\mu^- \to e^-\mu^-$ are connected with each other by $s \leftrightarrow u$ crossing. For the same reason the relation IV $\otimes A = -$III $\otimes A\,|_{s\to u}$ holds also for the expressions written in eqs.(15,18).

3.2 Infrared finiteness and numerical results

The infrared divergent terms proportional to ξ_{IR} in eqs.(27,28,31,33) follow again the pattern of the Born term $A'\otimes A'/t$. The leading order differential cross section gets therefore multiplied by the (infrared divergent) factor:

$$\begin{aligned}\delta_{\rm virt}^{(IR)} &= \frac{4\alpha}{\pi}\xi_{IR}\Bigg\{1+\frac{t-2}{\sqrt{4-t}}\,L(-t)+\frac{t-2r}{\sqrt{4r^2-rt}}\,L(-tr^{-1})\\ &\quad+{\rm Re}\Big[\frac{2(1+r-s)}{\sqrt{\rho_+-s}\sqrt{\rho_--s}}\ln\frac{\sqrt{\rho_+-s}+\sqrt{\rho_--s}}{2r^{1/4}}\Big]\\ &\quad+\frac{2(u-1-r)}{\sqrt{\rho_+-u}\sqrt{\rho_--u}}\ln\frac{\sqrt{\rho_+-u}+\sqrt{\rho_--u}}{2r^{1/4}}\Bigg\}. \end{aligned}\tag{34}$$

On the other hand, the (single) soft photon radiation from an electron or a muon yields the multiplicative factor:

$$\begin{aligned}\delta_{\rm soft} &= \alpha\,\mu^{4-d}\int_{|\vec{l}|<\lambda}\frac{d^{d-1}l}{(2\pi)^{d-2}\,l_0}\Big\{\frac{2p_1\cdot p_3}{p_1\cdot l\,p_3\cdot l}+\frac{2p_2\cdot p_4}{p_2\cdot l\,p_4\cdot l}+\frac{2p_1\cdot p_4}{p_1\cdot l\,p_4\cdot l}+\frac{2p_2\cdot p_3}{p_2\cdot l\,p_3\cdot l}\\ &\quad-\frac{2p_1\cdot p_2}{p_1\cdot l\,p_2\cdot l}-\frac{2p_3\cdot p_4}{p_3\cdot l\,p_4\cdot l}-\frac{m_e^2}{(p_1\cdot l)^2}-\frac{m_\mu^2}{(p_2\cdot l)^2}-\frac{m_e^2}{(p_3\cdot l)^2}-\frac{m_\mu^2}{(p_4\cdot l)^2}\Big\}, \end{aligned}\tag{35}$$

which includes exactly the same infrared divergence ($\sim \xi_{IR}$) but with the opposite sign. The remaining finite radiative correction factor for electron-muon scattering ($e^-\mu^- \to e^-\mu^-$) reads:

$$\begin{aligned}\delta_{\rm real}^{\rm (cm)} &= \frac{\alpha}{\pi}\Bigg\{4\Bigg[1+\frac{t-2}{\sqrt{4-t}}\,L(-t)+\frac{t-2r}{\sqrt{4r^2-rt}}\,L\Big(-\frac{t}{r}\Big)\\ &\quad+\frac{2}{\sqrt{P}}(s-1-r)\ln\frac{\sqrt{s-\rho_+}+\sqrt{s-\rho_-}}{2r^{1/4}}\\ &\quad+\frac{2(u-1-r)}{\sqrt{\rho_+-u}\sqrt{\rho_--u}}\ln\frac{\sqrt{\rho_+-u}+\sqrt{\rho_--u}}{2r^{1/4}}\Bigg]\ln\frac{m_\mu}{2\lambda}+\frac{2}{\sqrt{P}}\\ &\quad\times\Big[(s-1+r)\ln\frac{s-1+r+\sqrt{P}}{2\sqrt{sr}}+(s+1-r)\ln\frac{s+1-r+\sqrt{P}}{2\sqrt{s}}\Big]\\ &\quad+\int_0^{1/2}dx\Bigg[\frac{(t-2)(s+1-r)}{[1-tx(1-x)]\sqrt{R_t}}\ln\frac{s+1-r+\sqrt{R_t}}{s+1-r-\sqrt{R_t}}\\ &\quad+\frac{(t-2r)(s-1+r)}{[r-tx(1-x)]\sqrt{R_t}}\ln\frac{s-1+r+\sqrt{R_t}}{s-1+r-\sqrt{R_t}}\Bigg]\\ &\quad+\int_0^1 dx\Bigg[\frac{(s-1-r)[s+(1-r)(1-2x)]}{(1-2x)[sx(1-x)+(1-2x)(1-x-rx)]\sqrt{P}}\end{aligned}$$

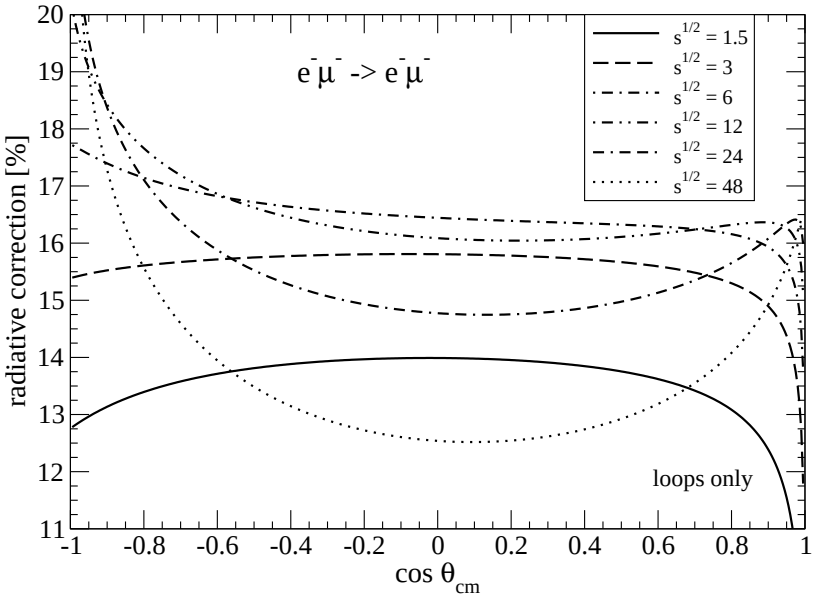

Figure 10: Radiative corrections to electron-muon scattering arising from loops only. The numbers $(1.5, 3, 6, 12, 24, 48)$ on the curves correspond to the total center-of-mass energy $\sqrt{s}m_\mu$ in units of m_μ.

$$\times \ln \frac{s+(1-2x)(1-r+\sqrt{P})}{s+(1-2x)(1-r-\sqrt{P})}$$
$$+\frac{(u-1-r)[s+(1-r)(1-2x)]}{[1+(r-1)x-ux(1-x)]\sqrt{R_u}} \ln \frac{s+(1-r)(1-2x)+\sqrt{R_u}}{s+(1-r)(1-2x)-\sqrt{R_u}} \Bigg] \Bigg\}, \qquad (36)$$

where we have introduced the polynomials: $P = s^2 - 2s(1+r) + (1-r)^2$, $R_t = P + 4stx(1-x)$, $R_u = P + 4x(1-x)[su - (1-r)^2]$. We note that the terms beyond those proportional to $\ln(m_\mu/2\lambda)$ are specific for the evaluation of the soft photon correction factor $\delta_{\rm soft}$ in the center-of-mass frame with λ an infrared cut-off therein. Setting $r = 1$ (i.e. $\rho_+ = 4$, $\rho_- = 0$) one recovers from eq.(36) the soft photon correction factor $\delta^{(\rm cm)}_{\rm real}$ for electron-electron scattering written in eq.(22).

Fig. 10 shows in percent the radiative corrections to electron-muon scattering arising from loops only (discarding the infrared divergence ξ_{IR}). A striking difference to the electron-electron case (see Fig. 4) is that these radiative corrections are now positive and larger in magnitude. Moreover, with increasing total center-of-mass energy $\sqrt{s}m_\mu$ the angular dependence of these radiative corrections changes. The maximum around $\theta_{\rm cm} \simeq 90^\circ$ turns gradually into a local minimum. At this point it should be stressed that these finite loop corrections are by themselves not physical since they have been obtained by dropping the (scheme-dependent) infrared divergence ξ_{IR}, which is defined here with the muon mass m_μ under the logarithm $\ln(m_\mu/\mu)$. When choosing a different mass scale, the loop corrections will change accordingly. The curves in Fig. 11 show the (full) radiative corrections to electron-muon scattering ($e^-\mu^- \to e^-\mu^-$) with inclusion of the soft photon bremsstrahlung. For the sake of having a concrete case we have set the infrared cutoff to the value $\lambda = \sqrt{s}m_\mu/200$. With inclusion of the soft photon bremsstrahlung the radiative corrections turn back to (sizeable) negative values and their energy and angular dependences follow more closely the pattern observed for electron-electron scattering (see Fig. 5). We do not discuss here in further detail the radiative corrections to electron-antimuon scattering $e^-\mu^+ \to e^-\mu^+$. These can be obtained through the crossing transformation ($s \leftrightarrow u$) in the loop amplitudes and a sign change in some interference terms of the soft photon correction factor $\delta_{\rm soft}$ (see eqs.(35,36)). For guidance one can compare eq.(22)

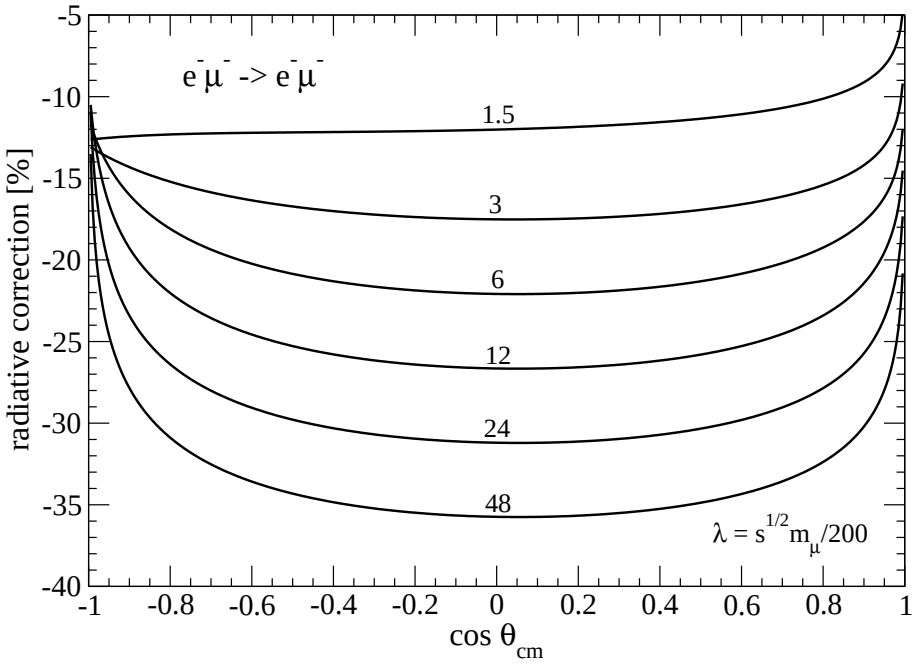

Figure 11: Radiative corrections to electron-muon scattering including soft photon bremsstrahlung. The numbers $(1.5, 3, 6, 12, 24, 48)$ on the curves correspond to the total center-of-mass energy $\sqrt{s}m_\mu$ in units of m_μ. The infrared cutoff has been set to $\lambda = \sqrt{s}m_\mu/200$.

with eq.(24) which exhibit this feature in the case of equal leptons.

3.3 Radiative corrections to lepton pair production

As a final application of our calculation we consider the radiative corrections to lepton pair production. The reaction $e^-(p_1) + e^+(p_2) \to \mu^+(p_3) + \mu^-(p_4)$ is obtained from electron-muon scattering via the crossing transformation $s \leftrightarrow t$. We define the center-of-mass scattering angle $\theta_{\rm cm}$ through the (uncrossed) variable $u = (p_1 - p_4)^2/m_\mu^2 = 1 + r + (\sqrt{s-4}\sqrt{s-4r}\cos\theta_{\rm cm} - s)/2$ as the angle between the momentum vectors of negatively charged particles. The differential and total cross section for $e^-e^+ \to \mu^+\mu^-$ at leading order have the following well-known form:

$$\frac{d\sigma^{(\rm pair)}}{d\Omega_{\rm cm}} = \frac{\alpha^2}{4m_\mu^2 s}\sqrt{\frac{s-4}{s-4r}}\left\{1 + \cos^2\theta_{\rm cm} + \frac{4}{s}(1+r)\sin^2\theta_{\rm cm} + \frac{16r}{s^2}\cos^2\theta_{\rm cm}\right\}, \tag{37}$$

$$\sigma_{\rm tot}^{(\rm pair)} = \frac{4\pi\alpha^2}{3m_\mu^2 s}\sqrt{\frac{s-4}{s-4r}}\left(1 + \frac{2}{s}\right)\left(1 + \frac{2r}{s}\right), \tag{38}$$

with $\sqrt{s}m_\mu$ the total center-of-mass energy and $r = (m_e/m_\mu)^2$.

The analytical expressions for the tree and loop contributions to lepton pair production $e^-e^+ \to \mu^+\mu^-$ can be directly taken over from eqs.(25-32) via the crossing transformation $s \leftrightarrow t$. However, the corresponding soft photon correction factor $\delta_{\rm soft}$, obtained formally from eq.(35) by the permutation $p_2 \leftrightarrow p_3$, needs to be reevaluated for the center-of-mass kinematics under consideration. After cancelling the infrared divergences ξ_{IR} against those from the loops the finite remainder of the soft photon correction factor for lepton pair production $e^-e^+ \to \mu^+\mu^-$ reads:

$$\delta_{\rm real}^{(\rm cm)} = \frac{\alpha}{\pi}\left\{4\left[1 + \frac{2-s}{\sqrt{s}}L(s-4) + \frac{2r-s}{\sqrt{sr}}L\Big(\frac{s}{r} - 4\Big)\right.\right.$$

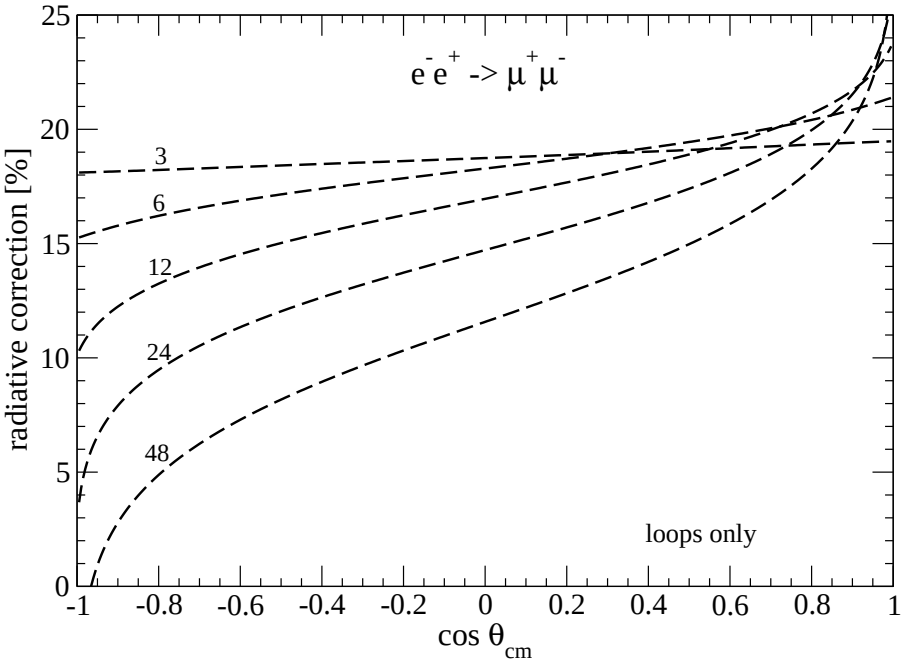

Figure 12: Radiative corrections to lepton-pair production $e^+e^- \to \mu^+\mu^-$ arising from photon loops only. The numbers $(3, 6, 12, 24, 48)$ on the curves correspond to the total center-of-mass energy $\sqrt{s}m_\mu$ in units of m_μ.

$$
\begin{aligned}
&+\frac{2(1+r-t)}{\sqrt{\rho_+ - t}\sqrt{\rho_- - t}} \ln \frac{\sqrt{\rho_+ - t} + \sqrt{\rho_- - t}}{2r^{1/4}} \\
&+\frac{2(u-1-r)}{\sqrt{\rho_+ - u}\sqrt{\rho_- - u}} \ln \frac{\sqrt{\rho_+ - u} + \sqrt{\rho_- - u}}{2r^{1/4}} \Bigg] \ln \frac{m_\mu}{2\lambda} \\
&+2\sqrt{\frac{s}{r}}\, L\Big(\frac{s}{r} - 4\Big) + 2\sqrt{s}\, L(s-4) \\
&+\int_0^{1/2} dx \Bigg[\frac{\sqrt{s}(2-s)(s-4)^{-1/2}}{(1-2x)[1+(s-4)x(1-x)]} \ln \frac{\sqrt{s} + (1-2x)\sqrt{s-4}}{\sqrt{s} - (1-2x)\sqrt{s-4}} \\
&+\frac{\sqrt{s}(2r-s)(s-4r)^{-1/2}}{(1-2x)[r+(s-4r)x(1-x)]} \ln \frac{\sqrt{s} + (1-2x)\sqrt{s-4r}}{\sqrt{s} - (1-2x)\sqrt{s-4r}} \Bigg] \\
&+\int_0^1 dx \Bigg[\frac{\sqrt{s}(1+r-t)}{[1+(r-1)x - tx(1-x)]\sqrt{C_t}} \ln \frac{\sqrt{s} + \sqrt{C_t}}{\sqrt{s} - \sqrt{C_t}} \\
&+\frac{\sqrt{s}(u-1-r)}{[1+(r-1)x - ux(1-x)]\sqrt{C_u}} \ln \frac{\sqrt{s} + \sqrt{C_u}}{\sqrt{s} - \sqrt{C_u}} \Bigg] \Bigg\}, \qquad (39)
\end{aligned}
$$

with the polynomials $C_t = s-4+4(1-r)x+4tx(1-x)$ and $C_u = s-4+4(1-r)x+4ux(1-x)$.

The dashed curves in Fig. 12 show the radiative corrections to muon pair production $e^-e^+ \to \mu^+\mu^-$ arising from loops only (discarding the infrared divergent terms ξ_{IR}). One notices that the forward-backward symmetry ($\theta_{\rm cm} \to 180^\circ - \theta_{\rm cm}$ or $t \leftrightarrow u$) of the tree level cross section (see eq.(37)) is broken by the loop corrections. This feature originates from the negative sign between the planar and crossed two-photon exchange contributions as exhibited in eq.(33) and explained afterwards. Also by interchanging the role of particle and antiparticle for μ^- and μ^+ one gets a relative minus sign between the one-photon and two-photon exchange contributions. Their (quantum mechanical) interference can therefore distinguish the two alternatives of fixing the scattering angle $\theta_{\rm cm}$ between the electron and μ^- direction or between the electron and μ^+ direction. This way a forward-backward asymmetry is generated by the two-photon exchange corrections. The full curves in Fig. 13 show the radiative corrections to muon pair production

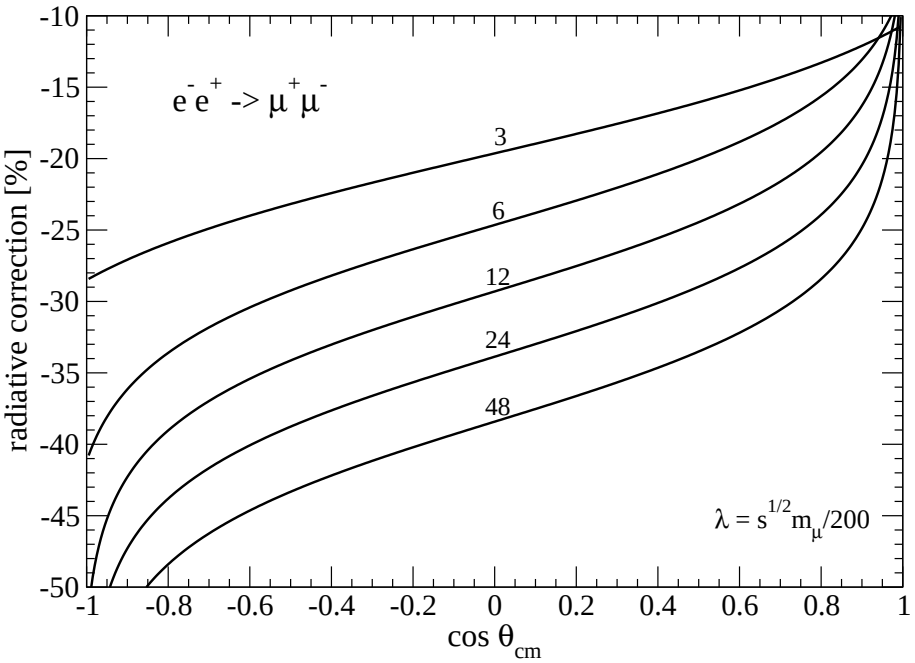

Figure 13: Radiative corrections to lepton-pair production $e^+e^- \to \mu^+\mu^-$ including soft photon bremsstrahlung. The numbers $(3, 6, 12, 24, 48)$ on the curves correspond to the total center-of-mass energy $\sqrt{s}m_\mu$ in units of m_μ. The infrared cutoff has been set to $\lambda = \sqrt{s}m_\mu/200$.

$e^-e^+ \to \mu^+\mu^-$ with inclusion of the soft photon bremsstrahlung. The infrared cutoff has been set to the value $\lambda = \sqrt{s}m_\mu/200$. One observes that the previous (scheme-dependent) positive radiative corrections from loops turn back into sizeable negative values by the soft photon bremsstrahlung. The forward-backward asymmetry becomes even more pronounced. The reason for that additional effect is that some interference terms of the soft photon emission are different for emission from positively and negatively charged muons. The expressions in the second and third as well as in the last two lines of eq.(39) demonstrate explicitly the asymmetry under $t \leftrightarrow u$ or equivalently $\cos\theta_{\rm cm} \to -\cos\theta_{\rm cm}$.

Finally, we show in Fig. 14 the radiative corrections to the total cross section for muon pair production $e^-e^+ \to \mu^+\mu^-$ as a function of the total center-of-mass energy $\sqrt{s}m_\mu$. In this case all t and u dependent contributions from two-photon exchange and soft photon bremsstrahlung (see eq.(39)) drop out, because they odd under $t \leftrightarrow u$ and thus integrate to zero. The analytical expression for the radiative corrections to the total cross section $\sigma_{\rm tot}(s)$ (see eq.(38)) can therefore be directly read off from eqs.(27-30) substituting $t \to s$, and from eq.(39) dropping the t and u dependent terms. The pertinent angular average of the Born term $A' \otimes A'$ for muon pair production $e^+e^- \to \mu^+\mu^-$ is of the form: $2(s+2)(s+2r)/3$.

This concludes our presentation and (schematic) discussion of the radiative corrections of order α to lepton-lepton scattering processes. It should be stressed again that for a comparison with real experiments the contributions from hard bremsstrahlung also have to be considered. The one-loop radiative corrections to muon-pair (and quark-pair) production in e^-e^+ collisions in the region of the Z^0-resonance have been calculated some time ago by Berends et al. in ref.[24]. The additional and new elements there are photonic vertex corrections to the Z^0-exchange and the γZ^0 box diagrams.

4 Radiative corrections to scalar boson scattering

For the sake of comparison, we treat in this section the radiative corrections to the scattering of (identical) charged scalar bosons. The new element in scalar quantum electrodynamics is

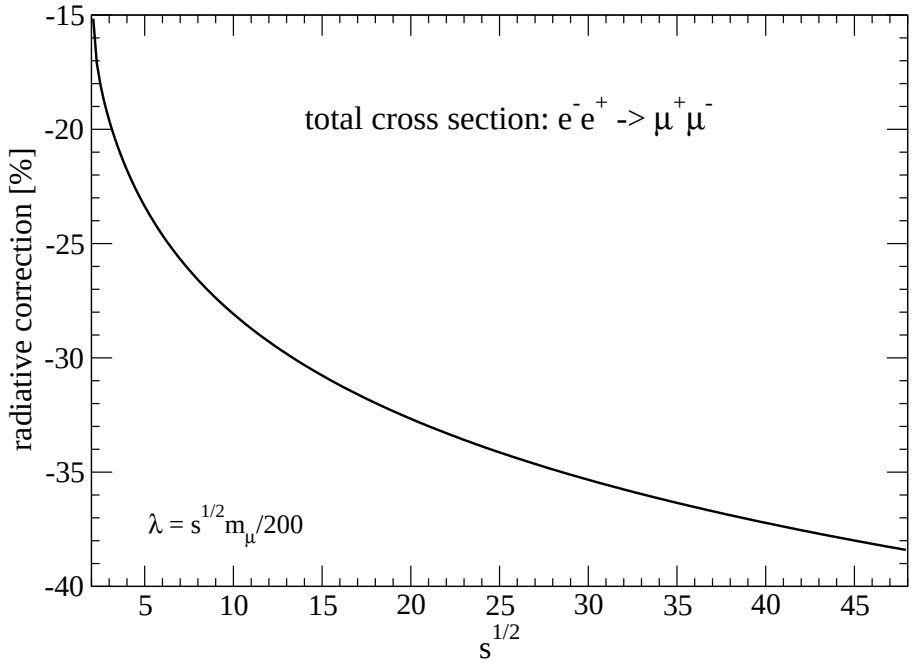

Figure 14: Radiative corrections to the total cross section for lepton pair production $e^+e^- \to \mu^+\mu^-$. The numbers $(3, 6, 12, 24, 48)$ on the curves correspond to the total center-of-mass energy $\sqrt{s}m_\mu$ in units of m_μ. The infrared cutoff has been set to $\lambda = \sqrt{s}m_\mu/200$.

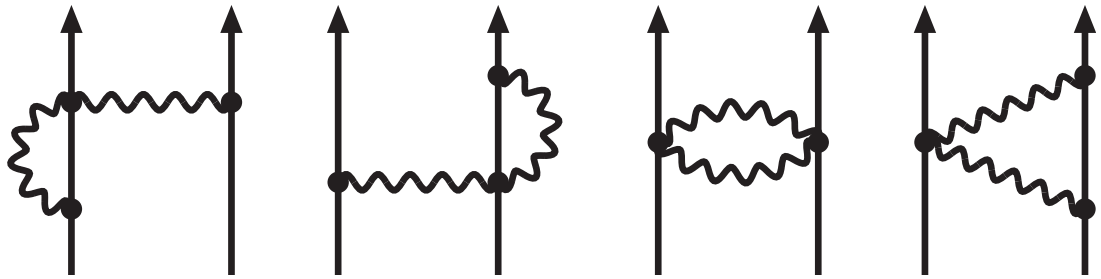

Figure 15: Additional (types of) photon-loop diagrams generated by the two-photon contact vertex of scalar quantum electrodynamics.

the two-photon contact vertex which generates several additional photon-loop diagrams.

In terms of the conventional (dimensionless) Mandelstam variables (s, t, u) the differential cross section for the reaction $b^-(p_1) + b^-(p_2) \to b^-(p_3) + b^-(p_4)$ takes the form:

$$\frac{d\sigma^{(b^-b^-)}}{d\Omega_{\rm cm}} = \frac{\alpha^2}{4m_b^2 s}\,|\mathcal{A}(t,u) + \mathcal{A}(u,t)|^2\,, \tag{40}$$

where $\mathcal{A}(t,u)$ is the scattering amplitude arising from diagrams with uncrossed (external) boson lines only. The corresponding tree-level Born term (as given by one-photon exchange) reads:

$$\mathcal{A}(t,u)^{(\rm tree)} = \frac{s-u}{t}\,. \tag{41}$$

Loop diagrams of scalar quantum electrodynamics contribute in the form of vertex corrections:

$$\mathcal{A}(t,u)^{(\rm vert)} = \frac{\alpha}{\pi t}(s-u)\Big\{2\xi_{IR} - 2 + \frac{t-2}{\sqrt{-t}\sqrt{4-t}}\Big[4(\xi_{IR}-1)\sqrt{-t}\,L(-t) + \Phi(-t)\Big]\Big\}\,, \tag{42}$$

and via a (scalar boson) vacuum polarization:

$$\mathcal{A}(t,u)^{(\rm vap)} = \frac{\alpha}{6\pi t^2}(s-u)\Big\{4 - \frac{4t}{3} - (4-t)^{3/2}L(-t)\Big\}\,. \tag{43}$$

Specific for scalar quantum electrodynamics are the two-photon exchange bubble and triangle diagrams shown in Fig.15. Their individual contributions to the scattering amplitude $\mathcal{A}(t,u)$ read:

$$\mathcal{A}(t,u)^{(\mathrm{bub})} = \frac{\alpha}{\pi}\Big\{ -4\xi_{UV} + 3 - 2\ln(-t)\Big\}\,, \tag{44}$$

$$\mathcal{A}(t,u)^{(\mathrm{tria})} = \frac{\alpha}{\pi}\Big\{2\xi_{UV} - 2 + 2\ln(-t) + (8-t)K(t)\Big\}\,. \tag{45}$$

with the function $K(t)$ defined in eq.(17) and ξ_{UV} denotes the ultraviolet divergence in dimensional regularization. Likewise, the planar two-photon exchange box diagram (see Fig. 3) for scalar bosons leads to the contribution:

$$\begin{aligned}\mathcal{A}(t,u)^{(\mathrm{box})} &= \frac{\alpha}{\pi}\Big\{\frac{1}{2}(1-\xi_{UV}) + \Big(3s - 8 + \frac{4s}{4-t}\Big)K(t) \\ &+\frac{4L(-s)}{t\sqrt{4-s}}\Big[\xi_{IR}(s-2)(u-s) - (s-2)^2\ln(-t)\Big] \\ &-\frac{1}{2}\sqrt{4-s}\,L(-s) - \frac{u\ln(-t)}{4-t} + \frac{(2-s)\,\Phi(-s)}{\sqrt{-s}\sqrt{4-s}}\Big\}\,,\end{aligned} \tag{46}$$

while that of the crossed two-photon exchange box diagram reads:

$$\begin{aligned}A(t,u)^{(\mathrm{crb})} &= \frac{\alpha}{\pi}\Big\{\frac{1}{2}(1-\xi_{UV}) + \Big(3u - 8 + \frac{4u}{4-t}\Big)K(t) \\ &+\frac{4L(-u)}{t\sqrt{4-u}}\Big[\xi_{IR}(u-2)(s-u) - (u-2)^2\ln(-t)\Big] \\ &-\frac{1}{2}\sqrt{4-u}\,L(-u) - \frac{s\ln(-t)}{4-t} + \frac{(2-u)\,\Phi(-u)}{\sqrt{-u}\sqrt{4-u}}\Big\}\,.\end{aligned} \tag{47}$$

As suggested by turning the charged boson line upside down, these last two contributions are related by the crossing transformation $s \leftrightarrow u$, i.e. $\mathcal{A}(t,u)^{(\mathrm{crb})} = \mathcal{A}(t,s)^{(\mathrm{box})}$ with $s = 4-t-u$. When summing the terms in eqs.(44-47) an ultraviolet divergence of $-3\alpha\,\xi_{UV}/\pi$ remains which in the end gets canceled by an appropriate counterterm of scalar quantum electrodynamics.

Fig. 16 shows the radiative corrections to equally charged scalar boson scattering arising from loops only. In comparison to the spin-1/2 case shown in Fig. 4, one observes that the transition from positive to negative loop corrections with increasing center-of-mass energy $\sqrt{s}m_b$ proceeds somewhat differently. The full lines in Fig. 17 show the radiative corrections with inclusion of the effects due to soft photon bremsstrahlung (given in identical form by eq.(22)). Altogether, one notices by comparison with Fig. 5 that the radiative corrections to the scattering of (equally charged) scalar bosons are somewhat smaller in magnitude than those for spin-1/2 fermions (at the same kinematical conditions).

Finally, we show in Figs. 18,19 the radiative corrections to the scattering of oppositely charged scalar bosons. As in the case of Bhabha scattering (see section 2.3) these are obtained through the crossing transformation $s \leftrightarrow u$ applied to the amplitude $\mathcal{A}(t,u)+\mathcal{A}(u,t)$ in eq.(40) and the corresponding soft photon correction factor $\delta^{(\mathrm{cm})}_{\mathrm{real}}$ is given by eq.(24). Making the comparison with Figs. 6,7 one is lead to the conclusion that for oppositely charged particles the radiative corrections are larger in magnitude for scalar bosons than for spin-1/2 fermions. Although not of direct practical relevance (since elementary charged scalar bosons do not exist in nature) this is an interesting observation.

In passing we note that the results obtained here in scalar QED cannot be applied e.g. to the pion. The electromagnetic form factor of the pion is dominated by the $\rho^0(770)$-resonance leading to an enhancement factor of up about 45 in the $\pi^+\pi^- \to \gamma^* \to \pi^+\pi^-$ transition (in the ρ^0 region). In addition, the hard part of the photon spectrum is radiated by quarks, not by the mesons themselves. Actually, the two-photon exchange contribution to the elastic electron-pion scattering has been calculated recently in ref. [25] taking into account the structure of the pion through a monopole-type (charge) form factor as suggested by vector-meson dominance model.

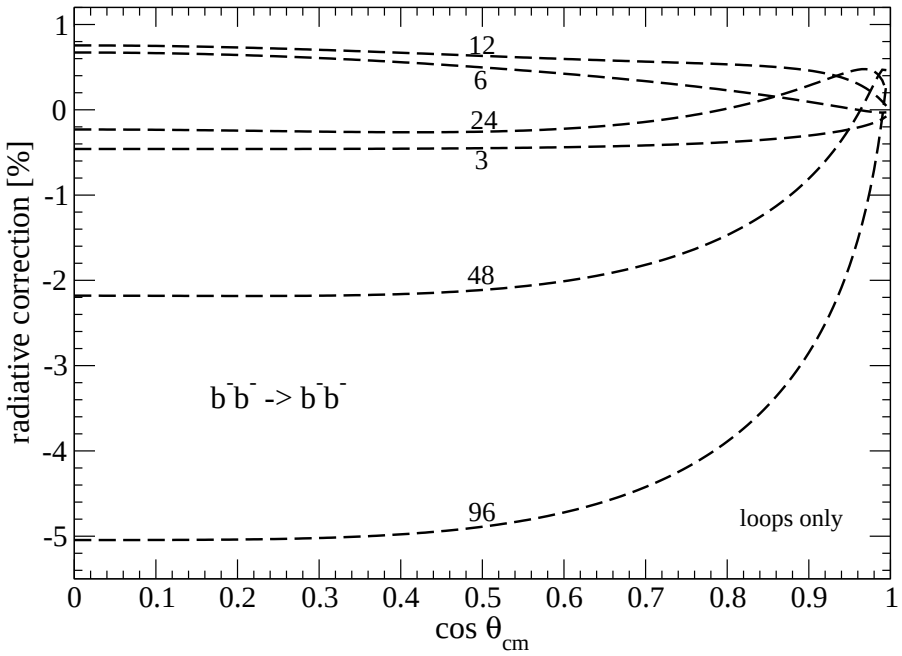

Figure 16: Radiative corrections to equally charged scalar boson scattering arising from loops only. The numbers $(3, 6, 12, 24, 48, 96)$ on the curves correspond to the total center-of-mass energy $\sqrt{s}m_b$ in units of m_b.

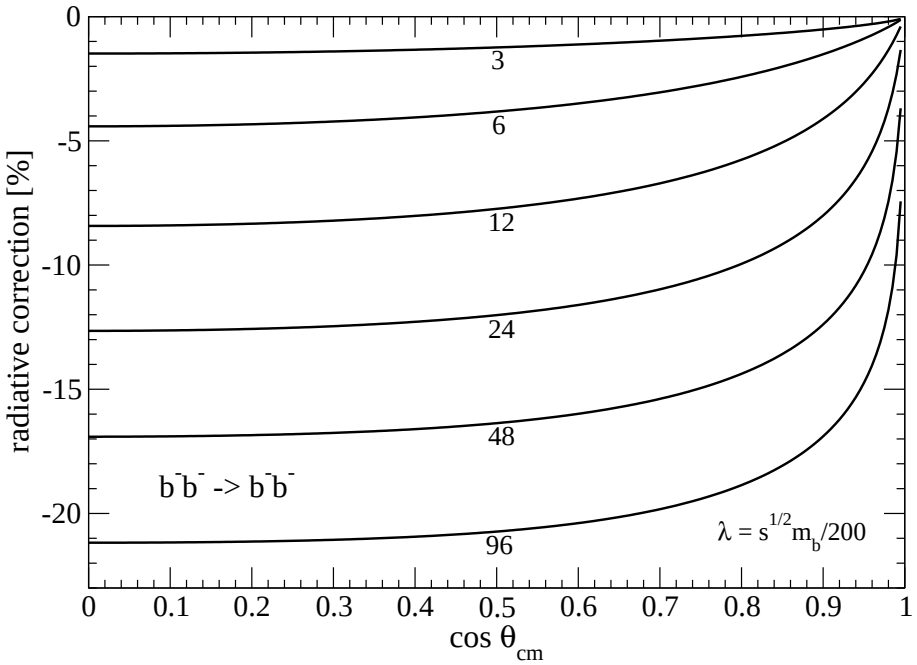

Figure 17: Radiative corrections to equally charged scalar boson scattering including soft photon bremsstrahlung. The numbers $(3, 6, 12, 24, 48, 96)$ on the curves correspond to the total center-of-mass energy $\sqrt{s}m_b$ in units of m_b. The infrared cutoff has been set to $\lambda = \sqrt{s}m_b/200$.

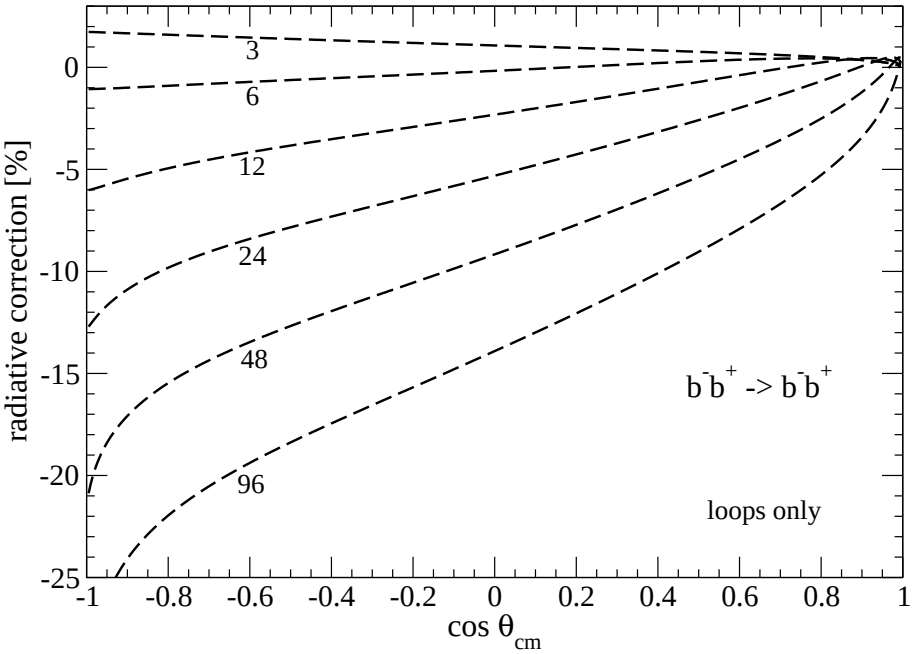

Figure 18: Radiative corrections to oppositely charged scalar boson scattering arising from loops only. The numbers $(3, 6, 12, 24, 48, 96)$ on the curves correspond to the total center-of-mass energy $\sqrt{s}m_b$ in units of m_b.

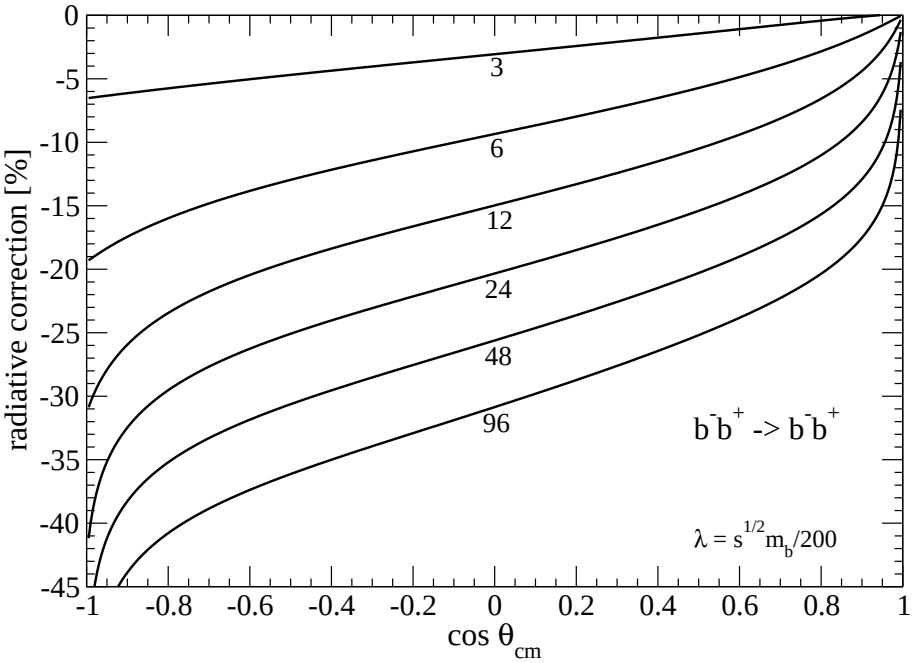

Figure 19: Radiative corrections to oppositely charged scalar boson scattering including soft photon bremsstrahlung. The numbers $(3, 6, 12, 24, 48, 96)$ on the curves correspond to the total center-of-mass energy $\sqrt{s}m_b$ in units of m_b. The infrared cutoff has been set to $\lambda = \sqrt{s}m_b/200$.

Appendix: Loop integrals

In this appendix we collect the results for the (basic) one-loop integrals one encounters in the calculation of the radiative corrections to lepton-lepton scattering. We are using dimensional regularization to treat both ultraviolet and infrared divergences. Divergent pieces of one-loop integrals show up in form of the constant:

$$\xi = \frac{1}{d-4} + \frac{1}{2}(\gamma_E - \ln 4\pi) + \ln\frac{m}{\mu}\,, \tag{48}$$

containing a simple pole at $d = 4$ and the logarithm of an arbitrary mass scale μ. Ultraviolet (UV) and infrared (IR) divergences are distinguished by the feature of whether $d < 4$ or $d > 4$ is the condition for convergence of the d-dimensional integral. In the following all propagators are understood to have an infinitesimal negative imaginary part: $-i0^+$.

The vacuum polarization diagram leads to the following loop integral with two (massive) propagators:

$$\int\frac{d^dl}{(2\pi)^di}\,\frac{(4\pi)^2\mu^{4-d}}{[m^2-l^2][m^2-(q-l)^2]} = I(t) + \mathcal{O}(d-4)\,, \tag{49}$$

where the dimensionless variable t is defined by $t\,m^2 = q^2$. In addition to the ultraviolet divergence $-2\xi_{UV}$ one obtains the logarithmic function:

$$I(t) = -2\xi_{UV} + 2 - \frac{2\sqrt{4-t}}{\sqrt{-t}}\ln\frac{\sqrt{4-t}+\sqrt{-t}}{2}\,, \tag{50}$$

whose imaginary part along the branch cut $t > 4$ is:

$$\mathrm{Im}\,I(t) = \frac{\pi\sqrt{t-4}}{\sqrt{t}}\,, \qquad \text{for} \quad t > 4\,. \tag{51}$$

The vertex correction diagram introduces the following loop integral with three propagators (two massive, one massless):

$$\int\frac{d^dl}{(2\pi)^di}\,\frac{(4\pi m)^2\mu^{4-d}}{[m^2-(p_1-l)^2][m^2-(p_2-l)^2][-l^2]} = H(t) + \mathcal{O}(d-4)\,, \tag{52}$$

where $t\,m^2 = (p_1-p_2)^2$ and $p_1^2 = p_2^2 = m^2$. The mass zero of the photon generates an infrared divergence ξ_{IR} and the complete result can be written as:

$$\begin{aligned} H(t) \;=\; & \frac{1}{\sqrt{-t}\sqrt{4-t}}\Big\{4\xi_{IR}\,\ln\frac{\sqrt{4-t}+\sqrt{-t}}{2} \\ & +\mathrm{Li}_2(v) - \mathrm{Li}_2(1-v) + \frac{1}{2}\ln^2 v - \frac{1}{2}\ln^2(1-v)\Big\}\,, \end{aligned} \tag{53}$$

in terms of logarithms and dilogarithms where $1-2v = \sqrt{-t/(4-t)}$. By convention, $\mathrm{Li}_2(v) = \sum_{n=1}^{\infty} n^{-2}v^n = v\int_1^\infty dy[y(y-v)]^{-1}\ln y$ denotes the dilogarithmic function. We note as an aside that when choosing a fictitious photon mass m_γ as an infrared regulator the infrared divergence appears always in the form $\xi_{IR} = \ln(m/m_\gamma)$. The imaginary part of $H(t)$ along the branch cut $t > 4$ is:

$$\mathrm{Im}\,H(t) = \frac{\pi}{\sqrt{t^2-4t}}\Big[2\xi_{IR} + \ln(t-4)\Big]\,, \qquad \text{for} \quad t > 4\,. \tag{54}$$

The two-photon exchange diagram introduces another loop integral with three propagators (one massive, two massless):

$$\int\frac{d^4l}{(2\pi)^4i}\,\frac{(4\pi m)^2}{[m^2-(p_1-l)^2][-(q-l)^2][-l^2]} = 2K(t)\,, \tag{55}$$

where $t\,m^2 = q^2 = 2p_1\cdot q$ and $p_1^2 = m^2$. Somewhat surprisingly, this loop integral is infrared convergent and the result has the analytical form:

$$K(t) = \frac{1}{\sqrt{-t}\sqrt{4-t}}\biggl\{\frac{\pi^2}{3} + \mathrm{Li}_2\Bigl(\frac{2-t-\sqrt{-t}\sqrt{4-t}}{2}\Bigr) + \ln^2\frac{\sqrt{4-t}+\sqrt{-t}}{2}\biggr\}. \tag{56}$$

The corresponding imaginary part along the cut $t > 0$ consists of two pieces:

$$\mathrm{Im}\,K(t) = \frac{\pi}{\sqrt{4t-t^2}}\,\arccos\frac{\sqrt{t}}{2}\,, \qquad \text{for} \quad 0 < t < 4\,, \tag{57}$$

$$\mathrm{Im}\,K(t) = \frac{\pi}{\sqrt{t^2-4t}}\,\ln\frac{\sqrt{t}+\sqrt{t-4}}{2}\,, \qquad \text{for} \quad t > 4\,, \tag{58}$$

which join smoothly at $t = 4$. Eventually, the two-photon exchange diagram leads to the following loop integral with four propagators (two massive, two massless):

$$\int\frac{d^dl}{(2\pi)^di}\,\frac{(4\pi m^2)^2\mu^{4-d}}{[m^2-(p_1-l)^2][m^2-(p_2+l)^2][-(q-l)^2][-l^2]} = \Psi(s,t) + \mathcal{O}(d-4)\,, \tag{59}$$

where the dimensionless variables (s,t) are defined by $s\,m^2 = (p_1+p_2)^2$, $t\,m^2 = q^2 = 2p_1\cdot q = -2p_2\cdot q$ and $p_1^2 = p_2^2 = m^2$. In analogy to eq.(44) the vanishing photon mass generates again an infrared divergence ξ_{IR} and the complete result reads:

$$\Psi(s,t) = \frac{4}{-t\,\sqrt{-s}\sqrt{4-s}}\Bigl[2\xi_{IR} + \ln(-t)\Bigr]\,\ln\frac{\sqrt{4-s}+\sqrt{-s}}{2}\,, \tag{60}$$

together with the imaginary part:

$$\mathrm{Im}\,\Psi(s,t) = \frac{2\pi}{-t\,\sqrt{s^2-4s}}\Bigl[2\xi_{IR} + \ln(-t)\Bigr]\,, \qquad \text{for} \quad s > 4\,,\;\; t < 0\,. \tag{61}$$

In the case of electron-muon scattering one encounters generalizations of the loop integrals $H(t)$ and $\Psi(s,t)$ (see eqs.(52,59)) with different masses $p_1^2 = m_e^2$ and $p_2^2 = m_\mu^2$ in the propagators and m_μ^2 in the numerator. The corresponding generalizations of the imaginary parts read:

$$\mathrm{Im}\,H_{e\mu}(t) = \frac{\pi}{\sqrt{(t-\rho_+)(t-\rho_-)}}\biggl\{2\xi_{IR} + \ln\frac{(t-\rho_+)(t-\rho_-)}{t}\biggr\}\,, \qquad \text{for} \quad t > \rho_+\,, \tag{62}$$

$$\mathrm{Im}\,\Psi_{e\mu}(s,t) = \frac{2\pi}{-t\,\sqrt{(s-\rho_+)(s-\rho_-)}}\Bigl[2\xi_{IR} + \ln(-t)\Bigr]\,, \qquad \text{for} \quad s > \rho_+\,,\;\; t < 0\,, \tag{63}$$

with $\rho_\pm = (1 \pm m_e/m_\mu)^2$. The importance of the imaginary parts of the loop functions lies in the fact that they determine via a Kramers-Kronig dispersion relation the corresponding real parts. On that basis we checked in detail (numerically) that the expressions with factorized square roots given in this appendix provide the correct analytical continuation of the real parts of the loop functions above their respective branch points.

The master integral occurring in the calculation of the soft photon correction factor δ_{soft} is:

$$\int_{-1}^{1}dx\,\frac{(1-x^2)^{\frac{d-4}{2}}}{(E+xp)^2} = \frac{2}{E^2-p^2}\biggl\{1 + (d-4)\Bigl[\ln 2 - \frac{E}{2p}\ln\frac{E+p}{E-p}\Bigr]\biggr\}\,, \tag{64}$$

carrying the expansion in $d-4$ up to linear order.

References

[1] J. Schwinger, *Phys. Rev.* **76**, 790 (1949).

[2] L.M. Brown and R.P. Feynman, *Phys. Rev.* **85**, 231 (1952).

[3] Y.S. Tsai, *Phys. Rev.* **122**, 1898 (1961).

[4] L.C. Maximon, *Rev. Mod. Phys.* **41**, 193 (1969).

[5] L.W. Mo and Y.S. Tsai, *Rev. Mod. Phys.* **41**, 205 (1969).

[6] P.A.M. Guichon and M. Vanderhaeghen, *Phys. Rev. Lett.* **91**, 142303 (2003).

[7] P.G. Blunden, W. Melnitchouk and J.A. Tjon, *Phys. Rev. Lett.* **91**, 142304 (2003).

[8] P.G. Blunden, W. Melnitchouk and J.A. Tjon, *Phys. Rev.* **C72**, 034612 (2005).

[9] J.A. Tjon, and W. Melnitchouk, *Phys. Rev. Lett.* **100**, 082003 (2008).

[10] J.A. Tjon, P.G. Blunden and W. Melnitchouk, *Phys. Rev.* **C79**, 055201 (2009)

[11] S. Kondratyuk, P.G. Blunden, W. Melnitchouk and J.A. Tjon, *Phys. Rev. Lett.* **95**, 172503 (2005).

[12] M. Vanderhaeghen, J.M. Friedrich, D. Lhuillier, D. Marchand, L. Van Hoorebeke and J. Van de Wiele, *Phys. Rev.* **C62**, 025501 (2000) .

[13] N. Kaiser and J.M. Friedrich, *Nucl. Phys.* **A812**, 186 (2008).

[14] N. Kaiser and J.M. Friedrich, *Eur. Phys. J.* **A39**, 71 (2009).

[15] G. Furlan and G. Peressutti, *Nuovo Cimento* **15**, 817 (1960).

[16] G. Furlan and G. Peressutti, *Nuovo Cimento* **19**, 830 (1961).

[17] Y.S. Tsai, *Phys. Rev.* **120**, 269 (1960).

[18] K.E. Eriksson, *Nuovo Cimento* **19**, 1029 (1961).

[19] K.E. Eriksson, *Nuovo Cimento* **21**, 383 (1961).

[20] K.E. Eriksson, B. Larsson and G.A. Rinander, *Nuovo Cimento* **30**, 1434 (1963).

[21] C. Itzykson and J.B. Zuber, Quantum Field Theory, McGraw-Hill book company, 1980; chapter 6.1.3.

[22] J. Fleischer, J. Gluza, A. Lorca and T. Riemann, *Eur. Phys. J.* **C48**, 35 (2006); and refs. therein.

[23] A.A. Penin, *Nucl. Phys.* **B743**, 185 (2006; and refs. therein).

[24] F.A. Berends, R. Kleiss and S. Jadach, *Nucl. Phys.* **B202**, 63 (1982).

[25] P.G. Blunden, W. Melnitchouk and J.A. Tjon, *Phys. Rev.* **C81**, 018202 (2010).